

Article

Discovery of the first-in-class dual histone deacetylase-proteasome inhibitor

Sanil Bhatia, Viktoria Krieger, Michael Groll, Jeremy Osko, Nina Reßing, Heinz Ahlert, Arndt Borkhardt, Thomas Kurz, David W. Christianson, Julia Hauer, and Finn K. Hansen

J. Med. Chem., **Just Accepted Manuscript** • DOI: 10.1021/acs.jmedchem.8b01487 • Publication Date (Web): 26 Oct 2018

Downloaded from <http://pubs.acs.org> on October 27, 2018

Just Accepted

“Just Accepted” manuscripts have been peer-reviewed and accepted for publication. They are posted online prior to technical editing, formatting for publication and author proofing. The American Chemical Society provides “Just Accepted” as a service to the research community to expedite the dissemination of scientific material as soon as possible after acceptance. “Just Accepted” manuscripts appear in full in PDF format accompanied by an HTML abstract. “Just Accepted” manuscripts have been fully peer reviewed, but should not be considered the official version of record. They are citable by the Digital Object Identifier (DOI®). “Just Accepted” is an optional service offered to authors. Therefore, the “Just Accepted” Web site may not include all articles that will be published in the journal. After a manuscript is technically edited and formatted, it will be removed from the “Just Accepted” Web site and published as an ASAP article. Note that technical editing may introduce minor changes to the manuscript text and/or graphics which could affect content, and all legal disclaimers and ethical guidelines that apply to the journal pertain. ACS cannot be held responsible for errors or consequences arising from the use of information contained in these “Just Accepted” manuscripts.



1
2
3
4
5
6
7
8
9
10
11
12
13
14
15
16
17
18
19
20
21
22
23
24
25
26
27
28
29
30
31
32
33
34
35
36
37
38
39
40
41
42
43
44
45
46
47
48
49
50
51
52
53
54
55
56
57
58
59
60

Discovery of the first-in-class dual histone deacetylase-proteasome inhibitor

Sanil Bhatia,^{‡,1} Viktoria Krieger,^{‡,2} Michael Groll,³ Jeremy D. Osko,⁴ Nina Reßing,⁵

Heinz Ahlert,¹ Arndt Borkhardt,¹ Thomas Kurz,² David W. Christianson,⁴ Julia Hauer^{,§,1}*

and Finn K. Hansen^{,§,5}*

¹Department of Pediatric Oncology, Hematology and Clinical Immunology, Medical

Faculty, Heinrich Heine University Düsseldorf, Moorenstr. 5, 40225 Düsseldorf,

Germany

²Institute for Pharmaceutical and Medicinal Chemistry, Heinrich Heine University

Düsseldorf, Universitätsstrasse 1, 40225 Düsseldorf, Germany

³Center for Integrated Protein Science at the Department Chemie, Lehrstuhl für

Biochemie, Technische Universität München, Lichtenbergstrasse 4, 85747 Garching,

Germany

1
2
3
4 ⁴Roy and Diana Vagelos Laboratories, Department of Chemistry, University of
5
6
7 Pennsylvania, 231 South 34th Street, Philadelphia, PA 19104-6323, United States
8
9

10
11 ⁵Pharmaceutical/Medicinal Chemistry, Institute of Pharmacy, Medical Faculty, Leipzig
12
13
14
15 University, Brüderstr. 34, 04103 Leipzig, Germany
16
17
18
19
20
21
22
23
24
25
26
27

28 29 **ABSTRACT**

30
31
32
33

34 Dual- or multi-target drugs have emerged as a promising alternative to combination
35
36
37 therapies. Proteasome inhibitors (PIs) possess synergistic activity with histone
38
39
40 deacetylase (HDAC) inhibitors due to the simultaneous blockage of the ubiquitin-
41
42
43 degradation and aggresome pathways. Here, we present the design, synthesis, binding
44
45
46 modes and anticancer properties of RTS-V5 as the first-in-class dual HDAC-proteasome
47
48
49 ligand. The inhibition of both targets was confirmed by biochemical and cellular assays
50
51
52
53
54
55 as well as X-ray crystal structures of the 20S proteasome and HDAC6 complexed with
56
57
58
59
60

1
2
3
4 RTS-V5. Cytotoxicity assays with leukemia and multiple myeloma cell lines as well as
5
6
7 therapy-refractory primary patient-derived leukemia cells demonstrated that RTS-V5
8
9
10 possesses potent and selective anticancer activity. Our results will thus guide the
11
12
13 structure-based optimization of dual HDAC-proteasome inhibitors for the treatment of
14
15
16
17 hematological malignancies.
18
19
20
21
22
23
24
25
26
27
28
29
30
31
32
33
34
35
36
37
38
39
40
41
42
43
44
45
46
47
48
49
50
51
52
53
54
55
56
57
58
59
60

INTRODUCTION

The approach “one drug multiple targets” or “multi-target drugs” is gaining major consideration in drug discovery and has been termed polypharmacology.¹ Despite the highly significant therapeutic relevance of combination therapies, potential advantages of a targeted therapy based on a single drug acting through two or more independent modes of action include (a) a more predictable pharmacokinetic profile, (b) increased patient compliance, and (c) the simultaneous presence of the molecule in tissues where the active principles are intended to work.¹

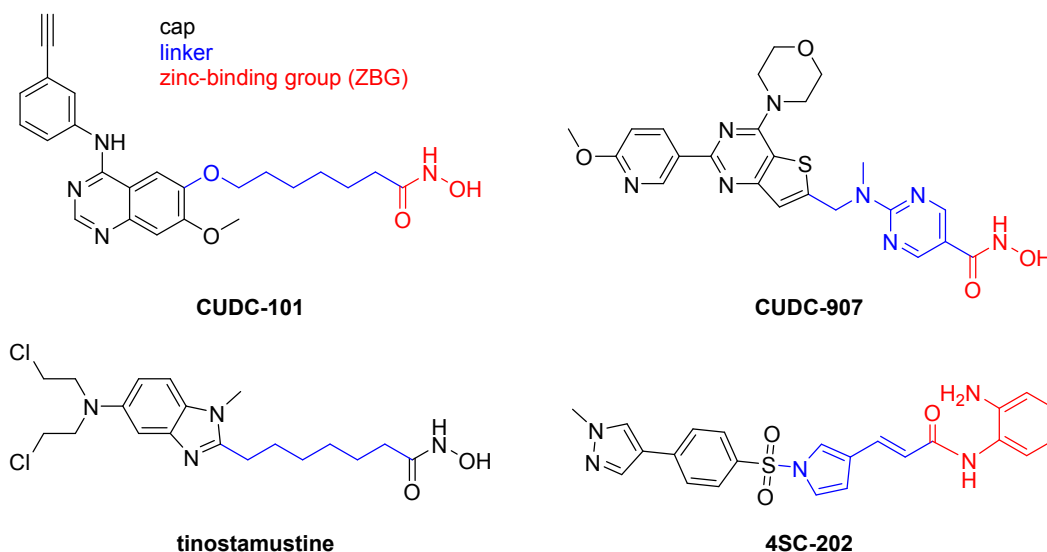


Figure 1. HDACi-based multi target drugs in clinical trials.

1
2
3
4
5
6
7 Histone deacetylases (HDACs) are clinically validated cancer targets and four inhibitors
8
9
10 thereof (HDACi) have been approved by the FDA for cancer therapy.² HDACi are
11
12
13 characterized by a cap-linker-zinc-binding group pharmacophore model (Figure 1).³
14
15
16
17 Fortunately, the HDACi pharmacophore tolerates a variety of cap groups which allows
18
19
20 scope for hybridization approaches.⁴ Consequently, the incorporation of a second
21
22
23
24 pharmacophore in the cap region has been used to engineer several HDACi-based multi-
25
26
27
28 target drugs.⁴ Notably, the dual kinase-HDAC inhibitors CUDC-101 and CUDC-907, the
29
30
31 nitrogen mustard-HDACi hybrid tinostamustine, as well as the dual LSD1-HDAC inhibitor
32
33
34
35 4SC-202, are currently being investigated in clinical trials (Figure 1).⁴⁻⁵ In regards to
36
37
38
39 combination therapy, the best investigated synergism of HDACi has been identified with
40
41
42
43 proteasome inhibitors (PIs) leading to dual proteasome and aggresome blockage and
44
45
46
47 apoptosis-induction due to the accumulation of misfolded proteins.⁶ However, to the best
48
49
50
51
52
53
54
55
56
57
58
59
60 of our knowledge, no dual HDAC-proteasome inhibitor has been reported so far.

1
2
3
4 Herein, we present the design, synthesis, biological evaluation, and binding modes of
5
6
7 RTS-V5 as the first-in-class dual HDAC-proteasome inhibitor.
8
9

10 11 12 RESULTS

13
14
15
16
17 **Design and synthesis of RTS-V5.** PIs can be divided into covalent and non-covalent
18
19
20 binders.⁷ We decided to focus on non-covalent scaffolds to suppress several drawbacks
21
22
23 such as excessive reactivity, lack of specificity, and/or stability.⁸ Moreover, highly reactive
24
25
26 electrophilic warheads might cause chemical incompatibilities with the typical HDACi zinc-
27
28
29 binding groups (ZBGs) such as hydroxamic acids, aminoanilides or thioles. The first non-
30
31
32 covalent acting PI was identified in the crystal structure of the yeast proteasome in
33
34
35 complex with the natural product TMC-95A.⁹ In the following years, binding modes of
36
37
38 TMC-95A derivatives¹⁰ as well as non-covalent linear peptide mimetics have been
39
40
41
42 reported.¹¹ In particular, a promising PI turned out to be compound ML16 (Figure 2)
43
44
45
46
47
48 obtained from an elaborate study published by Blackburn and colleagues.^{11a} The high
49
50
51
52 affinity of ML16 and several analogs is primarily achieved by a P3-neopentyl-Asn residue
53
54
55
56
57
58
59
60 (Figure 2). The comparison of currently available crystal structures of the proteasome in

1
2
3
4 complex with peptidic ligands¹² revealed that this bulky residue indeed represents a
5
6
7 superb side chain to occupy the entire S3 specificity pocket of the chymotrypsin-like site
8
9
10 of the 20S core particle. We, therefore, decided to use ML16 as a starting point for the
11
12
13 design of dual HDAC-proteasome inhibitors. The S4 binding site does not resemble a
14
15
16 pocket-like structure and a careful inspection of a series of X-ray structures of ML16 and
17
18
19 its analogs indicated that the P4 residue is solvent exposed.^{7, 11a} As a result, we aimed at
20
21
22 the design of a HDAC-proteasome hybrid inhibitor by incorporating the HDACi part at the
23
24
25 P4 position (Figure 2). The most obvious synergy between PIs and HDACi is derived from
26
27
28 the inhibition of HDAC6.^{6, 13} Thus, we chose an *N*-hydroxybenzamide scaffold as HDACi
29
30
31 part as this moiety provides HDAC6 selectivity.¹⁴
32
33
34
35
36
37
38
39
40
41
42
43
44
45
46
47
48
49
50
51
52
53
54
55
56
57
58
59
60

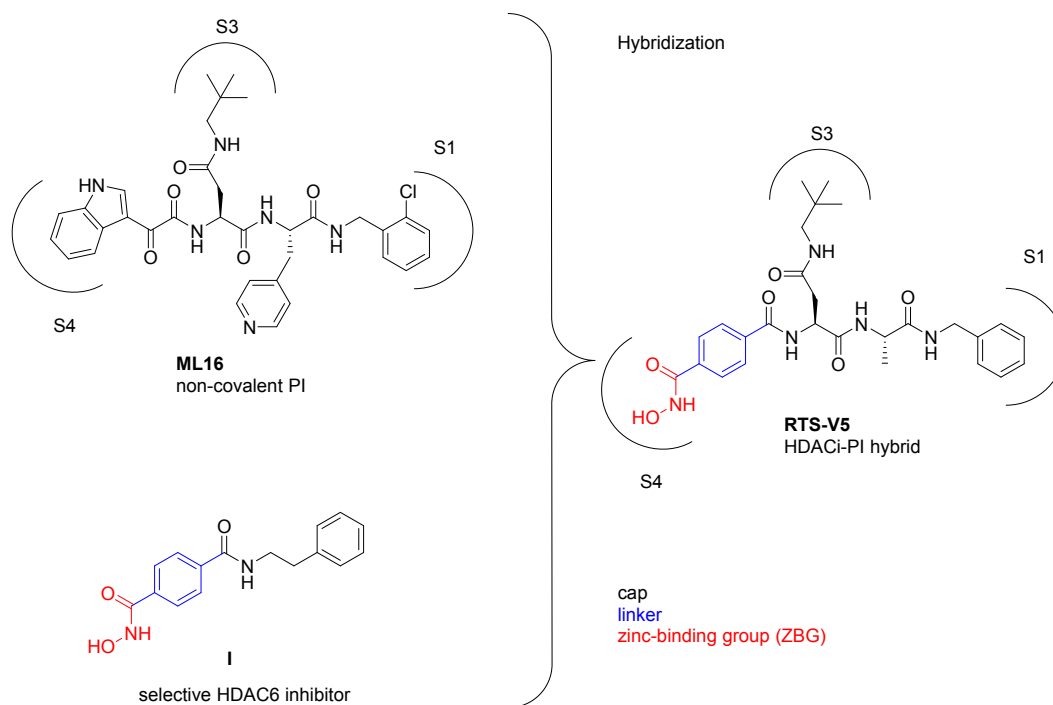


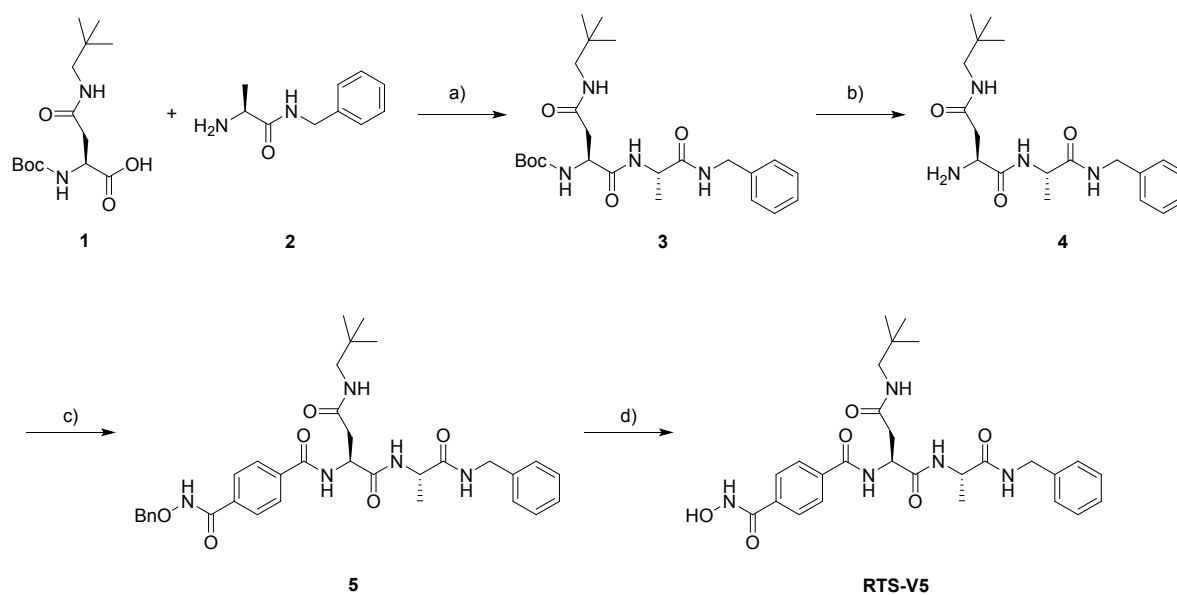
Figure 2. Design of RTS-V5 as the first-in-class dual HDAC-proteasome inhibitor.

Compound I (Figure 2) is a representative example of a selective HDAC6 inhibitor based on an *N*-hydroxybenzamide group. Furthermore, the solvent-exposed 4-picolyl group in the P2 position was replaced by a methyl group in order to reduce the molecular weight of the hybrid compound. Our hybridization strategy thus yielded the prototype HDAC-proteasome hybrid inhibitor RTS-V5 (Figure 2).

RTS-V5 was synthesized as outlined in Scheme 1. The readily available building blocks 1 and 2 were combined by HATU-mediated coupling to generate dipeptide 3. Next, the

1
2
3
4 deprotection of **3**, followed by introduction of 4-((benzyloxy)carbonyl)benzoic acid via
5
6
7 another amide coupling reaction afforded the protected hydroxamic acid **5**. Finally,
8
9
10 catalytic hydrogenolysis of **5** provided the target compound RTS-V5.
11
12
13
14
15
16
17
18
19

20 Scheme 1. Synthesis of RTS-V5.^a



^aReagents and conditions: a) HATU, DIPEA, DMF, rt, 16 h. b) TFA, CH₂Cl₂, rt, 4 h. c) 4-
((Benzyloxy)carbonyl)benzoic acid, HATU, DIPEA, DMF, rt, 24 h. d) Pd/C, H₂, rt, 4 h.

1
2
3 **RTS-V5 inhibits histone deacetylase and proteasomal activity.** RTS-V5 was evaluated
4
5
6
7 for its ability to inhibit both histone deacetylase and proteasomal activity. First, we tested
8
9
10 the compound in a biochemical assay for activity against recombinant HDAC6. The
11
12
13 screening demonstrated potent submicromolar activity with an IC_{50} value of 0.27 μ M
14
15
16
17 (Figure 3a). To assess the selectivity of RTS-V5 for HDAC6, it was further tested for
18
19
20 activity against all class I isoforms (HDACs 1, 2, 3, and 8, Figure 3a). Our analysis
21
22
23 revealed that RTS-V5 has low activity against HDACs 1, 2, and 3. However, HDAC8 was
24
25
26
27 blocked at submicromolar concentrations as well (HDAC8 IC_{50} : 0.53 μ M) which can be
28
29
30
31 explained by the lowered rim of the catalytic channels of HDAC6 and HDAC8.¹⁵
32
33
34
35
36
37
38
39
40
41
42
43
44
45
46
47
48
49
50
51
52
53
54
55
56
57
58
59
60

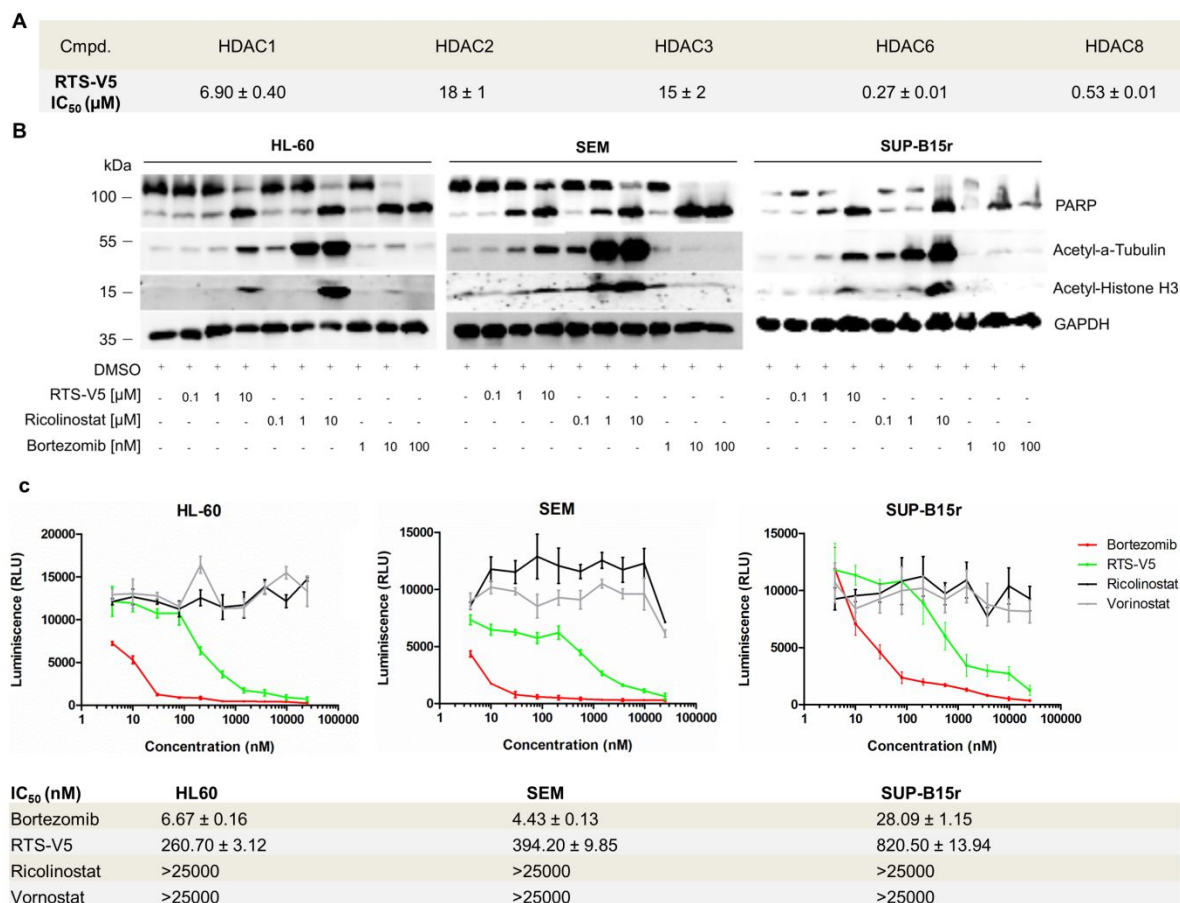


Figure 3. Functional specificity of RTS-V5 against HDAC6 and the proteasome. a)

Inhibitory activities of compounds RTS-V5 against HDAC isoforms 1, 2, 3, 6, and 8. b),

HL-60, SEM, and SUP-B15r cells were exposed to bortezomib, vorinostat, ricolinostat,

and RTS-V5 at the indicated concentration for 24 h, after which lysates were

immunoblotted with anti-acetyl- α -tubulin, anti-acetyl-Histone H3, poly (ADP-ribose)

polymerase (PARP), and anti-glycerinaldehyd-3-phosphat-dehydrogenase (GAPDH)

antibodies. c) HL-60, SEM, and SUP-B15r cells were treated for 2 h with bortezomib,

1
2
3 vorinostat, ricolinostat and RTS-V5 at concentrations ranging from 4 nM-25 μ M. The
4
5
6
7 proteasomal activity was measured after 2 h using the cell-based Proteasome-Glo
8
9
10 Chymotrypsin-Like assay by taking Suc-LLVY-aminoluciferin (Succinyl-leucine-leucine-
11
12
13
14 valine-tyrosine-aminoluciferin) as a substrate. The compounds were printed on a 384-
15
16
17 well plate using a randomization feature (n = 3).
18
19
20
21
22
23

24 In the following, we aimed to evaluate the inhibition of RTS-V5 against HDAC6 in a
25
26
27 cellular environment. Therefore, we treated the acute myeloid leukemia (AML) cell line
28
29
30
31 HL-60 as well as the B-cell precursor acute lymphoblastic leukemia (BCP-ALL) cell lines
32
33
34 SEM and SUP-B15r (Tyrosine Kinase Inhibitor (TKI) - resistant)¹⁶ with RTS-V5, the
35
36
37 preferential HDAC6 inhibitor ricolinostat and the FDA-approved proteasome inhibitor
38
39
40
41 bortezomib for 24 h. Next, the cell lysates were immunoblotted with anti-acetyl- α -tubulin
42
43
44
45 and acetyl-Histone H3 antibodies (Figure 3b). Compared to bortezomib, the treatment
46
47
48
49 with RTS-V5 enhanced the expression of acetyl- α tubulin and acetyl-histone H3 in
50
51
52
53 accordance to ricolinostat. Furthermore, RTS-V5 upregulated the expression of cleaved
54
55
56
57
58
59
60

1
2
3 PARP, a marker of apoptosis, corresponding to ricolinostat and bortezomib (Figure 3b).

4
5
6
7 The inhibition of proteasome activity by RTS-V5 was evaluated using a cell-based
8
9
10 chymotrypsin-like Glo assay (Promega) by taking bortezomib as a positive control and
11
12
13 ricolinostat (HDAC6i) or vorinostat (pan-HDACi) as a negative marker (Figure 3c). In all
14
15
16 selected leukemic cell lines (HL-60, SEM and SUP-B15r), RTS-V5 blocked the
17
18
19 chymotrypsin-like proteasome activity while vorinostat and ricolinostat were unable to
20
21
22 inhibit the protease. Furthermore, it was shown that RTS-V5 acts specifically on the
23
24
25 chymotrypsin-like activity, i.e. RTS-V5 was unable to inhibit the trypsin- and caspase-like
26
27
28 proteasome activities (Figure S1a, S1b, Supporting Information). Thus, these results
29
30
31 demonstrate that RTS-V5 is the first-in-class dual HDAC-proteasome inhibitor.
32
33
34
35
36
37
38

39 **Co-crystal structures of RTS-V5 in complex with HDAC6 and the 20S proteasome.**

40
41
42 Encouraged by the functional specificity of RTS-V5 against HDAC6 and the proteasome,
43
44
45 we set out to elucidate its binding modes in the vastly differing targets. First, the crystal
46
47
48 structure of catalytic domain 2 (CD2) of *Danio rerio* (zebrafish) HDAC6 complexed with
49
50
51 RTS-V5 was determined at 1.90 Å resolution ($R_{\text{free}} = 0.190$, PDB ID: 6CW8, Table S1,
52
53
54
55
56
57
58
59
60

1
2
3 Supporting Information). The crystal structures of zebrafish and human CD2 enzymes are
4
5
6 identical,^{17a} so zebrafish HDAC6 CD2 (henceforth simply "HDAC6") serves as a more
7
8
9 readily studied surrogate of the human enzyme. The crystal structure of the enzyme-
10
11
12 inhibitor complex depicts no major conformational changes between the inhibitor-bound
13
14
15
16
17 and unliganded states of the enzyme, and the root-mean-square (rms) deviation is 0.14
18
19
20 Å for 287 C α atoms (unliganded HDAC6, PDB accession code 5EEM). Notably, there are
21
22
23 two independent and essentially identical monomers in this crystal form (rms deviation =
24
25
26
27 0.15 Å for 299 C α atoms). Electron density for RTS-V5 is generally well defined in both
28
29
30
31 monomers (monomer A, Figure 4; monomer B, Figure S2, Supporting Information).
32
33
34 Enzyme-inhibitor interactions are quite similar in both monomers, except for alternative
35
36
37 interactions resulting from individual conformations of the benzyl-L-alanyl moiety in
38
39
40
41 monomers A and B, respectively (Figure S3, Supporting Information).
42
43
44
45
46
47
48
49
50
51
52
53
54
55
56
57
58
59
60

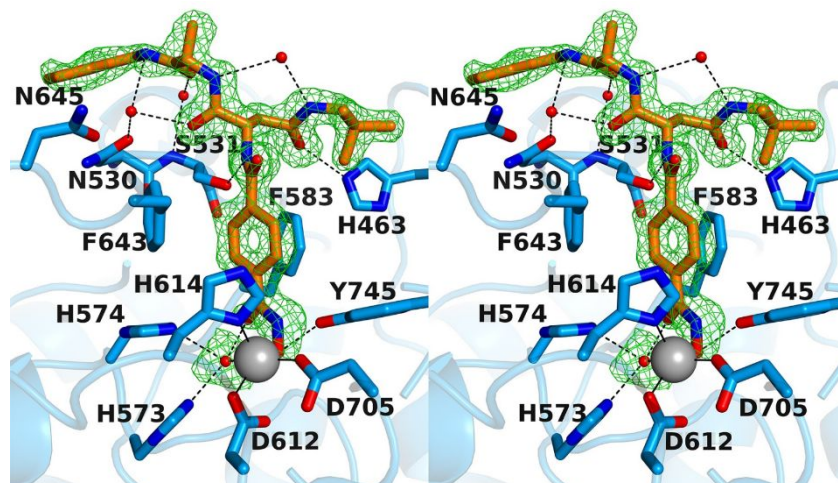


Figure 4. Stereoview of the Polder omit map of RTS-V5 bound to monomer A of HDAC6 (contoured at 3.0σ) (PDB ID 6CW8). Atoms are color-coded as follows: C = orange (RTS-V5) or light blue (protein), N = blue, O = red, Zn^{2+} = gray sphere, solvent = red spheres. Metal coordination and hydrogen bond interactions are indicated by solid and dashed black lines, respectively. The Zn^{2+} coordination geometry is pentacoordinate square pyramidal.

In both monomers, the hydroxamate moiety of RTS-V5 coordinates to the active site Zn^{2+} ion in monodentate fashion, in a similar manner to that observed in complexes with other bulky phenylhydroxamate inhibitors such as HPOB, HPB, and ACY-1083.¹⁷ This binding mode is characterized by the coordination of the ionized hydroxamate hydroxyl

1
2
3 group to Zn^{2+} (average $\text{Zn}^{2+}\text{---O}$ separation = 2.0 Å), while the hydroxamate carbonyl
4
5
6
7 group accepts a hydrogen bond from a Zn^{2+} -bound water molecule (average $\text{O}\text{---O}$
8
9
10 separation = 2.8 Å). The Zn^{2+} -bound N-O^- group also accepts a hydrogen bond from Y745
11
12
13 (average $\text{O}\text{---O}$ separation = 2.6 Å).
14
15
16
17

18 Beyond the Zn^{2+} coordination polyhedron, intermolecular interactions observed for
19
20
21
22 RTS-V5 in both monomers contribute to inhibitor affinity and selectivity. The aromatic ring
23
24
25 of the phenylhydroxamate is sandwiched between two fully conserved residues, F583
26
27
28 and F643. The *para*-substituted amide NH group forms a hydrogen bond with S531 on
29
30
31 the L2 loop (average $\text{N}\text{---O}$ separation = 3.0 Å). Notably, S531 is unique to HDAC6 and
32
33
34 plays an important role in substrate binding.^{17a} Thus, hydrogen bonds with S531
35
36
37
38
39 presumably contribute to HDAC6 inhibitor selectivity.
40
41
42
43

44 In monomer A, the carbonyl group of the neopentylamide moiety accepts a hydrogen
45
46
47 bond from H463 in the L1 loop with an $\text{O}\text{---N}$ separation of 2.9 Å; in monomer B, the $\text{O}\text{---}$
48
49
50 N separation is 3.3 Å, which is slightly too long for, but perhaps within experimental error
51
52
53
54
55
56
57
58
59
60

of, a hydrogen bond. Interestingly, H463 is unique to vertebrate HDAC6 isozymes, so this interaction may confer additional selectivity toward HDAC6.

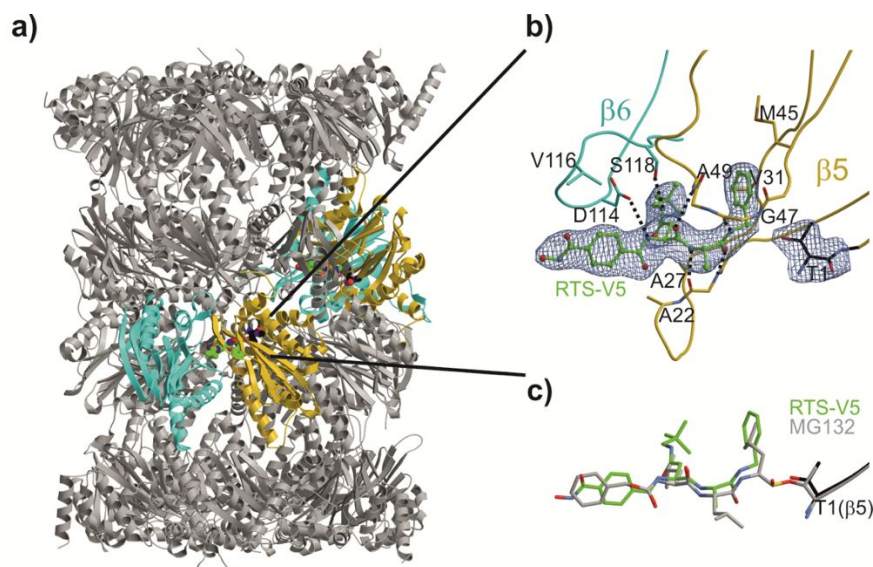


Figure 5. Yeast 20S proteasome in complex with RTS-V5. **a)** Cartoon representation of the yeast 20S proteasome core particle (yCP) in complex with RTS-V5 (PDB ID: 6H39). The decarboxylated ligand is presented as a sphere model, which is located at the intersection of the β - β' -rings. The molecule solely binds to the nonprimed substrate binding channel of the chymotrypsin-like active site, which is composed of subunits $\beta 5$ (gold) and $\beta 6$ (cyan), respectively. **b)** The $2F_{\text{O}}-F_{\text{C}}$ electron density map of the non-covalent inhibitor is illustrated as blue mesh and contoured to 1σ . Hydrogen bonds

1
2
3 forming the antiparallel β -sheet between ligand and protein main chain residues are
4
5
6 indicated by black dashed lines. RTS-V5 intensely interacts with the S1 and S3 sites,
7
8
9
10 whereas the P2-Ala side chain is solvent-exposed. Amino acid numbering is according to
11
12
13 Löwe et al.¹⁸ and Groll et al.¹⁹. c) Structural superposition of RTS-V5 with the covalently
14
15
16 acting aldehyde inhibitor MG132 (PDB ID: 4NNN)²⁰ depicts a uniform arrangement. The
17
18
19
20
21
22
23
24
25
26
27
28
29
30
31
32
33
34
35
36
37
38
39
40
41
42
43
44
45
46
47
48
49
50
51
52
53
54
55
56
57
58
59
60

hemiacetal bond is highlighted in gold.

Next, the crystal structure of the yeast 20S proteasome core particle (yCP) in complex
with RTS-V5 was determined to 2.5 Å resolution ($R_{\text{free}} = 0.217$, PDB ID: 6H39, Table S2,
Supporting Information). Intriguingly, the $2F_{\text{O}}-F_{\text{C}}$ electron density map displays the entire
inhibitor molecule only bound to the chymotrypsin-like active site by adopting an
antiparallel β -sheet structure (Figure 5a, b). Importantly, the HDACi hydroxamic acid ZBG
of RTS-V5 is solvent exposed and thus, not in contact with protein residues. In agreement
with our predictions, the complex structure depicts that the ligand acts non-covalently on
the proteasome. Compared to standard inhibitors bound to the CP, such as the tripeptide
aldehyde MG132,²⁰ our study revealed that RTS-V5 is solely stabilized by Van der Waals

1
2
3 interactions with its P1 benzene ring to Val31, Ala49 and predominantly Met45 of subunit
4
5
6 β 5, while its P3-neopentyl-Asn-moiety forms elaborate interactions with $\gamma\beta$ 5-Ala49 as well
7
8
9
10 as Asp114, Val116 and Ser118 of $\gamma\beta$ 6 (Figure 5b, c). Notably, the electron density map
11
12
13 uncovered the presence of an *N*-morpholino-ethane-sulfonic acid molecule (MES) in
14
15
16
17 proximity to the inhibitor, which is derived from the crystallization buffer. Hereby, the
18
19
20 sulfonate moiety of MES interacts with β 5Gly47NH and hence, occupies the oxyanion
21
22
23 hole, an area normally populated by the active residue of ligands such as i) the oxygen
24
25
26
27 anion of the scissile peptide bond in its tetrahedral intermediate,²¹ or ii) functional groups
28
29
30
31 of covalently bound inhibitors.²² Taken together, the crystallographic insights at the
32
33
34
35 molecular resolution confirmed our structure-activity relationships demonstrating that the
36
37
38 non-covalent proteasome inhibitor RTS-V5 fulfils elaborate interactions with the distinct
39
40
41
42 specificity pockets of the chymotrypsin-like substrate binding channel, hereby generating
43
44
45 target specificity.
46
47
48
49

50 **Specific cytotoxic activity of RTS-V5 against cancerous cells.** In order to investigate the
51
52
53 anticancer properties of our dual HDAC-proteasome inhibitor, RTS-V5 was screened for
54
55
56
57
58
59
60

1
2
3
4 cytotoxicity against a panel of leukemia and multiple myeloma cell lines using ricolinostat
5
6
7 as a positive control (Table 1). Hereby, RTS-V5 showed comparable or higher cytotoxicity
8
9
10 than ricolinostat with IC_{50} values in the single-digit micromolar to submicromolar
11
12
13 concentration range. The highest activity of RTS-V5 was observed against the BCP-ALL
14
15
16 cell line SEM (IC_{50} : 0.89 μ M). Our dual inhibitor was also active against TKI-resistant
17
18
19 SUP-B15r and KCL-22r cells¹⁶ with IC_{50} values of 1.83 and 2.58 μ M, respectively (Table
20
21
22
23
24 1). Due to its encouraging activity against chemosensitive and chemoresistant BCP-ALL
25
26
27 cell lines, RTS-V5 was further tested for activity against primary BCP-ALL cells derived
28
29
30 from four therapy-refractory patients (Patient 1 and 2 from initial diagnosis and Patient 3
31
32
33 and 4 from the relapse cohort) revealing IC_{50} values ranging from 1.51 to 5.23 μ M (Table
34
35
36
37
38 1).

39
40
41
42
43 Next, we evaluated the cell viability in peripheral blood derived mononuclear cells
44
45
46 (PBMCs) from healthy individuals. Strikingly, RTS-V5 showed only marginal toxicity
47
48
49 against PBMCs (IC_{50} >25 μ M, Figure S4, Supporting Information). In contrast, the
50
51
52 reference compounds ricolinostat, vorinostat and bortezomib caused significant
53
54
55
56
57
58
59
60

1
2
3
4 cytotoxicity against PBMCs with IC₅₀ values in the single-digit micromolar (ricolinostat,
5
6
7 vorinostat) or even submicromolar concentration range (bortezomib) (Figure S4,
8
9
10 Supporting Information). These data emphasize that RTS-V5 possesses promising
11
12
13 anticancer properties against several leukemic and multiple myeloma cell lines as well as
14
15
16 patient-derived BCP-ALL cells. Intriguingly, RTS-V5 acts in an encouraging therapeutic
17
18
19
20
21 window.

22
23
24
25 **Table 1.** Cytotoxicity of RTS-V5 and ricolinostat against selected leukemia and multiple
26
27
28 myeloma cell lines as well as patient-derived BCP-ALL cells.

29
30
31
32

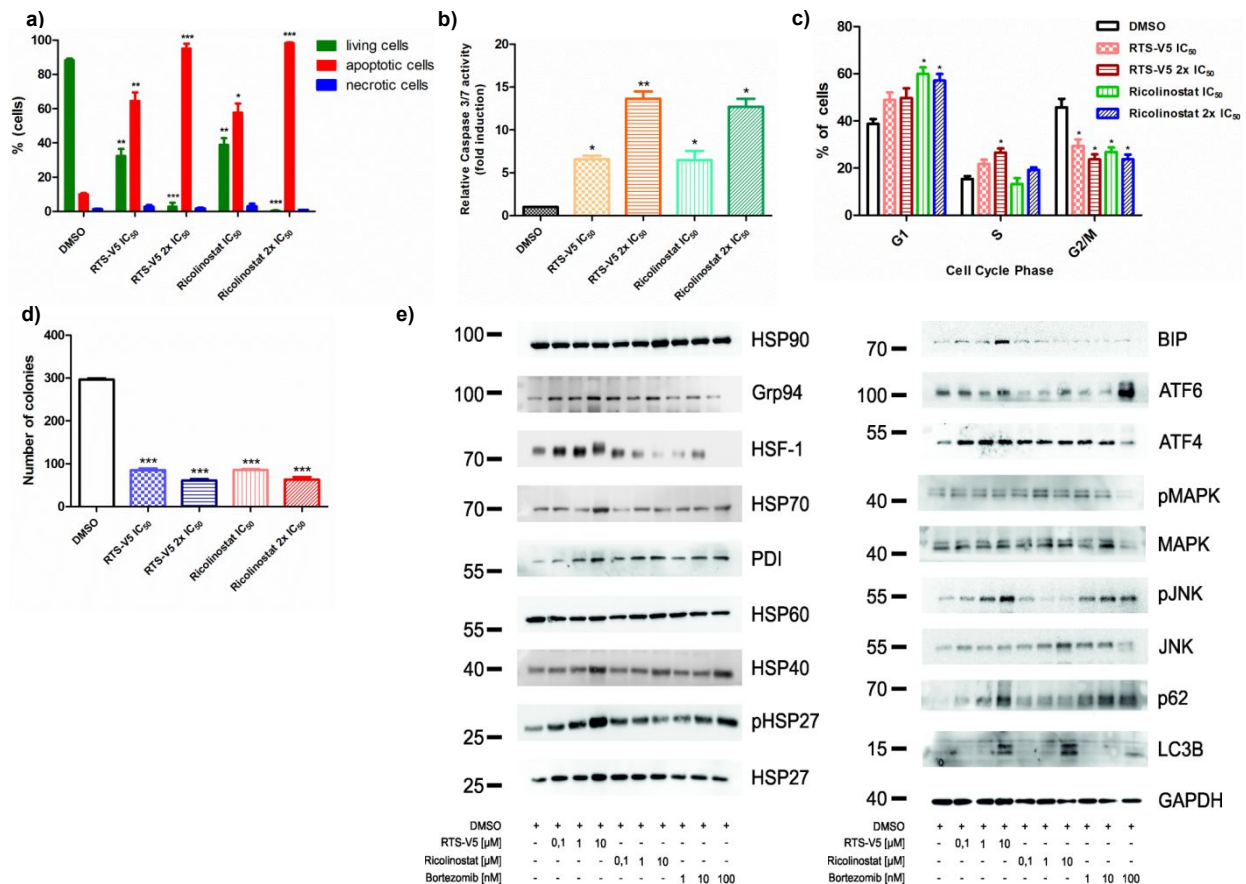
Cell line	Characteristic	RTS-V5 IC ₅₀ [μM]	Ricolinostat IC ₅₀ [μM]
HL60	AML ^a	1.55 ± 0.02	2.36 ± 0.07
SEM	BCP-ALL ^b	0.89 ± 0.01	1.61 ± 0.02
SUP-B15	BCP-ALL ^b	1.77 ± 0.02	1.92 ± 0.07
KCL-22	CML ^c	3.14 ± 0.03	3.75 ± 0.09
SUP-B15r	BCP-ALL ^{b,d}	1.83 ± 0.03	3.54 ± 0.02
KCL-22r	CML ^{c,d}	2.58 ± 0.04	3.38 ± 0.03
RPMI-8226	MM ^e	1.75 ± 0.32	1.97 ± 0.12
U266	MM ^e	2.04 ± 0.37	3.52 ± 0.38
Patient 1	BCP-ALL ^b	2.06 ± 0.16	0.29 ± 0.01
Patient 2	BCP-ALL ^b	1.84 ± 0.07	0.58 ± 0.04
Patient 3	BCP-ALL ^b	5.23 ± 0.13	4.45 ± 0.14
Patient 4	BCP-ALL ^b	1.51 ± 0.05	0.54 ± 0.01

33
34
35
36
37
38
39
40
41
42
43
44
45
46
47
48
49
50
51
52
53
54
55
56
57
58
59
60

1
2
3
4 ^aAcute myeloid leukemia. ^bB-cell precursor acute lymphoblastic leukemia. ^cChronic
5
6
7 myeloid leukemia. ^dImatinib resistant. ^eMultiple myeloma.
8
9

10
11 Based on these promising results, the biological properties of RTS-V5 were analyzed
12 in more detail using the BCP-ALL cell line SEM. RTS-V5 significantly inhibited the
13
14 proliferation of SEM cells at its IC₅₀ or 2x IC₅₀ concentrations, comparable to ricolinostat
15
16
17
18 (Figure S5, Supporting Information). RTS-V5 induced apoptosis in SEM cells as
19
20
21
22
23
24
25
26
27
28
29
30
31
32
33
34
35
36
37
38
39
40
41
42
43
44
45
46
47
48
49
50
51
52
53
54
55
56
57
58
59
60
SEM cells significantly reduced their colony forming capacity (Figure 6d). In addition,

1
2
3 exposure of RTS-V5 to SEM cells induces the heat shock response or HSR (marked by
4
5
6 the overexpression of Grp94, HSP70, HSP40, and HSP27 proteins), unfolded protein
7
8 response or UPR (marked by the overexpression of BIP, ATF4, ATF6, and pJNK proteins)
9
10
11 in response to combat the proteotoxic stress and autophagy (marked by the
12
13
14
15
16
17
18 overexpression of LC3B and p62 proteins) (Figure 6e).



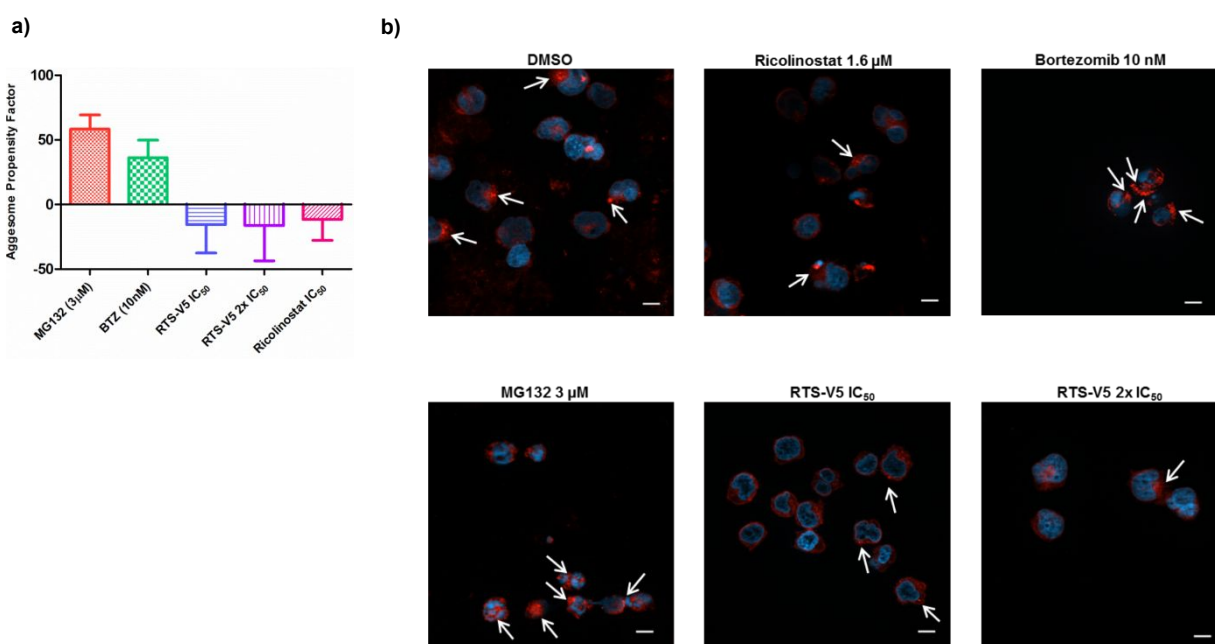
1
2
3 **Figure 6.** RTS-V5 as a potent inhibitor in a leukemic cell line. **a)** SEM cells were treated
4 with RTS-V5 and ricolinostat at IC_{50} or at $2x IC_{50}$ concentration for 48 h. Subsequently
5
6 with RTS-V5 and ricolinostat at IC_{50} or at $2x IC_{50}$ concentration for 48 h. Subsequently
7
8 dual staining was performed with annexin V/PI and measured by FACS. Viable cells (-ve
9
10 for annexin V/PI) were analyzed if they are necrotic (+ve for PI) and are either in an early
11
12 (+ve for annexin V) or in a late (+ve for both annexin/PI) apoptotic stage. The bar graph
13
14 is depicting the percentage of living, apoptotic and necrotic cells after 48 h exposure to
15
16 RTS-V5 or ricolinostat. **b)** SEM cells were treated with RTS-V5 for 48 h followed by
17
18 determining the enzymatic activity of caspase 3/7 by applying a Glo assay (absorbance
19
20 at 405 nm) to record the induction of apoptosis. **c)** SEM cells were treated with RTS-V5
21
22 for 48 h, and after propidium iodide staining cell cycle analysis was carried out by FACS.
23
24
25
26
27
28
29
30
31
32
33
34
35
36
37
38 **d)** SEM cells were seeded in a semisolid methylcellulose-based medium after 48 h
39
40 treatment with RTS-V5 or controls. Next, the impact of RTS-V5 on the differentiation
41
42 ability of leukemic cells was evaluated. The bar-graphs depict the colonies counted after
43
44
45
46
47
48
49
50
51
52
53
54
55
56
57
58
59
60 **e)** SEM cells were treated with bortezomib, ricolinostat, and RTS-V5 at the
indicated concentration for 18 h, after which the expression of proteins involved in the
HSR, UPR and autophagy were analyzed by western blot analyses. The achieved values

1
2
3 depicted in the Figure 5 are plotted as a bar graph. Columns depict the mean of 3
4
5
6
7 independent experiments (n = 3). Significance analyses of normally distributed data with
8
9
10 variance similar between groups used paired, two-tailed student's t-test. * p < 0.05, ** p
11
12
13 < 0.005, *** p < 0.001.
14
15
16
17
18
19
20

21 Aggresomes are inclusion bodies produced in response to inhibition of the ubiquitin-
22
23
24 proteasome machinery. HDAC6 together with the motor protein dynein is required to
25
26
27 recruit cytotoxic, ubiquitylated proteins to aggresomes. The effect of RTS-V5 on the
28
29
30 aggresome accumulation was studied using fluorescence microscopy and FACS upon
31
32
33 staining with an aggresome dye (Figure 7a, b). The well-known proteasome inhibitors
34
35
36 MG132 and bortezomib were used as positive controls whereas ricolinostat served as
37
38
39 negative control. RTS-V5 significantly blocked aggresome accumulation at its inhibitory
40
41
42 concentration as opposed to bortezomib and MG132, but in accordance with ricolinostat.
43
44
45
46
47
48
49

50 These results led us to conclude that RTS-V5 induces apoptosis and blocks
51
52
53 proliferation, cell cycle, colony formation, and aggresome accumulation in the SEM cell
54
55
56
57
58
59
60

1
2
3 line. Furthermore, the exposure of RTS-V5 leads to the activation of HSR and UPR.
4
5
6
7 Hence, our findings together with the crystallographic and biochemical data demonstrate
8
9
10 that RTS-V5 eradicates cancer cells by dual blockage of the aggresome-proteasome
11
12
13
14 pathway.
15
16
17
18



42 **Figure 7.** Effect of RTS-V5 on the aggresome accumulation. **a)** SEM cells were treated
43 with the respective compounds at their indicated concentration for 18 h. In the following,
44 the Enzo proteostat aggresome detection kit was used to stain the cells along with their
45 DNA. Pictures were taken with a 63X objective using fluorescence microscopy. Scale =
46
47
48
49 the Enzo proteostat aggresome detection kit was used to stain the cells along with their
50
51
52 DNA. Pictures were taken with a 63X objective using fluorescence microscopy. Scale =
53
54
55
56 10 μ m. **b)** Treated SEM cells were analyzed by FACS upon staining with aggresome dye
57
58
59
60

1
2
3 to determine the aggresome propensity factor according to the relative mean
4
5
6
7 fluorescence intensity (MFI).
8
9
10
11
12

13 DISCUSSION AND CONCLUSIONS

14
15
16
17

18 The 'one-disease-one-drug' paradigm has dominated drug development strategies for
19
20 decades.²³ However, the so-called magic bullets, molecules that exhibit high selectivity
21
22 and potency for one target, are often not effective to treat multifactorial diseases such as
23
24 cancer or neurological disorders.^{4a} Consequently, combination therapy is a cornerstone
25
26 of cancer therapy: the combination of anti-cancer drugs enhances efficacy compared to
27
28 the mono-therapy approach because it modulates key pathways in an additive or even
29
30 synergistic manner.²⁴ Bortezomib is often given in combination with the pan-HDACi
31
32 panobinostat. The combination of HDAC6i and proteasome inhibitors leads to increased
33
34 α -tubulin acetylation as well as to accumulation of misfolded proteins.²⁵ Misfolded
35
36 proteins accumulate because both clearance routes, the proteasome and the aggresome
37
38 pathway, are blocked; in turn, this leads to apoptosis of the cell.²⁶ Thus, the simultaneous
39
40
41
42
43
44
45
46
47
48
49
50
51
52
53
54
55
56
57
58
59
60

1
2
3 inhibition of both pathways could be of high clinical importance to combat hematological
4
5
6
7 malignancies.
8
9

10
11 A phase I/II trial conducted for patients with relapsed or refractory multiple myeloma
12
13 showed that therapy with ricolinostat as a single agent resulted in neither significant
14
15 toxicity nor clinical responses.²⁷ However, combination therapy with the proteasome
16
17 inhibitor bortezomib and dexamethasone achieved a response rate of 37%.²⁷ Similar
18
19 results were reported in a study using a combination therapy including the proteasome
20
21 inhibitor MG132 and vorinostat, which induced synergistic cytotoxicity in leukemia cells
22
23 by downregulating BCR-ABL1 expression and by inducing intracellular ROS levels.²⁸
24
25
26
27
28
29
30
31
32
33
34
35
36

37 In recent years, multi-target drugs have emerged as a powerful alternative to
38
39 combination chemotherapy. Although several HDACi-based multi-target drugs have been
40
41 described before, it is surprising that no dual HDAC-proteasome inhibitors have been
42
43 reported to date. In this work, we have designed and synthesized RTS-V5 as a first-in-
44
45 class dual HDAC-proteasome inhibitor. We have shown that this compound inhibits both
46
47
48
49
50
51 HDAC6 and the chymotrypsin-like proteasome activity. RTS-V5 induces apoptosis, HSR,
52
53
54
55
56
57
58
59
60

1
2
3 UPR and autophagy in the SEM cell line. Furthermore, it blocks cell cycle, colony
4
5
6
7 formation, and aggresome accumulation. It is an encouraging finding that RTS-V5
8
9
10 displayed potent anticancer activity against a panel of chemosensitive, chemoresistant
11
12
13 leukemic and multiple myeloma cell lines, as well as against therapy-refractory primary
14
15
16 patient-derived leukemia cells without imposing toxicity against PBMC cells from healthy
17
18
19
20
21 volunteers. In future studies the efficacy and toxicity of RTS-V5 or improved analogues
22
23
24 will be investigated in *in vivo* models in comparison to a combination treatment with a
25
26
27 HDAC6 inhibitor and a proteasome inhibitor (e.g. ricolinostat combined with bortezomib)
28
29
30
31 in order to further evaluate the therapeutic potential of this promising new class of multi-
32
33
34 target ligands.
35
36
37
38

39 To the best of our knowledge, this is also the first report of a dual target binder with
40
41
42 accompanying co-crystal structures of complexes with both protein targets. The X-ray
43
44
45 structures confirmed several important features that might lead to fewer side effects. The
46
47
48 non-covalent and selective inhibition of chymotrypsin-like proteasome activity may
49
50
51 explain the selective toxicity profile of RTS-V5 compared to covalent proteasome
52
53
54
55
56
57
58
59
60

1
2
3 inhibitors such as bortezomib.¹² Selective HDAC6 inhibition is clinically preferable since
4
5
6
7 there is growing evidence that there are intrinsic toxic side effects associated with
8
9
10 inhibition of HDAC1-3.²⁹ The monodentate zinc-binding observed for RTS-V5 can be
11
12
13 exploited by bulky phenylhydroxamate-based HDACi. However, binding of these
14
15
16
17 inhibitors in the sterically constricted active site of HDAC1-3 would be disfavored.^{17b} Thus,
18
19
20
21 the monodentate zinc-binding mode is believed to contribute to the significantly reduced
22
23
24 inhibition of HDAC1-3 and low toxicity of RTS-V5 compared to the pan-inhibitor vorinostat.
25
26
27
28 Moreover, our determined crystal structures of RTS-V5 in complex with HDAC6 and the
29
30
31 20S proteasome will ultimately pave the way for the structure-based optimization of dual
32
33
34 HDAC-proteasome inhibitors for advanced preclinical studies.
35
36
37
38

39 EXPERIMENTAL SECTION

40 41 42 43 44 Chemistry

45
46
47
48 *General.* All reagents and solvents were purchased from commercial sources and used
49
50
51 without further purification. Thin layer chromatography was carried out using Macherey-
52
53
54 Nagel pre-coated aluminium foil sheets which were visualised using UV light (254 nm)
55
56
57
58
59
60

1
2
3 and, in the case of hydroxamic acids, stained with a 1% solution of iron(III) chloride in
4
5
6
7 methanol. $^1\text{H-NMR}$ and $^{13}\text{C-NMR}$ spectra were recorded at room temperature on Bruker
8
9
10 Avance III HD (400 MHz), Bruker Avance III (600 MHz), Bruker Avance DRX (500 MHz)
11
12
13 and Varian/Agilent Mercury-plus (300 MHz) spectrometers. Chemical shifts (δ) are quoted
14
15
16 in parts per million (ppm). All spectra were standardised in accordance with the signals
17
18
19 of the deuterated solvent ($\text{DMSO-}d_6$: $\delta_{\text{H}} = 2.50$ ppm; $\delta_{\text{C}} = 39.5$ ppm). Coupling constants
20
21
22 (J) are reported in Hertz (Hz). Mass-spectra were measured by the Leipzig University
23
24
25
26
27
28 Mass Spectrometry Service, using electrospray ionisation (ESI) on a Bruker Daltonics
29
30
31 ESI-TOF micrOTOF. The uncorrected melting points were determined using a Barnstead
32
33
34 Electrothermal 9100 apparatus. Analytical HPLC analysis were carried out using a
35
36
37
38 Knauer Azura P 6.1L system equipped with P 6.1L (pumps), a Smartline UV detector
39
40
41
42 2600 and a Phenomenex Luna 5u C18(2) 1.8 μm particle (250 mm x 4.6 mm) column,
43
44
45 supported by Phenomenex Security Guard Cartridge Kit C18 (4.0 mm x 3.0 mm). UV
46
47
48 absorption was detected at 254 nm with a linear gradient of 10% B to 100% B within 20
49
50
51 min. HPLC-grade water (solvent A) and HPLC-grade acetonitrile (solvent B) were used
52
53
54
55 for elution at a flow rate of 1 mL/min. Both solvents were enriched with 0.1% TFA. The
56
57
58
59
60

1
2
3
4 purity of the final compound was at least 95%. The synthesis of 4-
5
6
7 ((benzyloxy)carbamoyl)benzoic acid is described in the Supporting Information.
8
9

10
11 *tert*-Butyl ((*S*)-1-(((*S*)-1-(benzylamino)-1-oxopropan-2-yl)amino)-4-(neopentylamino)-
12
13
14
15 **1,4-dioxobutan-2-yl)carbamate (3)**. *tert*-Butyl (*S*)-(1-benzylamino)-1-oxopropan-2-
16
17
18 yl)carbamate (6.64 g, 23.85 mmol, 1 eq) was dissolved in a mixture of trifluoroacetic
19
20
21 acid/CH₂Cl₂ (1:2, 30 mL) and stirred at room temperature for 4 h. After completion of the
22
23
24
25 reaction, the solution was basified (pH ≈ 9) using sat. sodium carbonate solution. The
26
27
28
29 mixture was extracted with CH₂Cl₂ (3 x 20 mL) and washed with 1M sodium hydroxide
30
31
32
33 solution (3 x 20 mL) and brine (3 x 20 mL). Subsequently, the collected organics were
34
35
36
37 dried over sodium sulfate and the solvent was removed under reduced pressure to yield
38
39
40
41
42
43
44
45
46
47
48
49
50
51
52
53
54
55
56
57
58
59
60
61
62
63
64
65
66
67
68
69
70
71
72
73
74
75
76
77
78
79
80
81
82
83
84
85
86
87
88
89
90
91
92
93
94
95
96
97
98
99
100
101
102
103
104
105
106
107
108
109
110
111
112
113
114
115
116
117
118
119
120
121
122
123
124
125
126
127
128
129
130
131
132
133
134
135
136
137
138
139
140
141
142
143
144
145
146
147
148
149
150
151
152
153
154
155
156
157
158
159
160
161
162
163
164
165
166
167
168
169
170
171
172
173
174
175
176
177
178
179
180
181
182
183
184
185
186
187
188
189
190
191
192
193
194
195
196
197
198
199
200
201
202
203
204
205
206
207
208
209
210
211
212
213
214
215
216
217
218
219
220
221
222
223
224
225
226
227
228
229
230
231
232
233
234
235
236
237
238
239
240
241
242
243
244
245
246
247
248
249
250
251
252
253
254
255
256
257
258
259
260
261
262
263
264
265
266
267
268
269
270
271
272
273
274
275
276
277
278
279
280
281
282
283
284
285
286
287
288
289
290
291
292
293
294
295
296
297
298
299
300
301
302
303
304
305
306
307
308
309
310
311
312
313
314
315
316
317
318
319
320
321
322
323
324
325
326
327
328
329
330
331
332
333
334
335
336
337
338
339
340
341
342
343
344
345
346
347
348
349
350
351
352
353
354
355
356
357
358
359
360
361
362
363
364
365
366
367
368
369
370
371
372
373
374
375
376
377
378
379
380
381
382
383
384
385
386
387
388
389
390
391
392
393
394
395
396
397
398
399
400
401
402
403
404
405
406
407
408
409
410
411
412
413
414
415
416
417
418
419
420
421
422
423
424
425
426
427
428
429
430
431
432
433
434
435
436
437
438
439
440
441
442
443
444
445
446
447
448
449
450
451
452
453
454
455
456
457
458
459
460
461
462
463
464
465
466
467
468
469
470
471
472
473
474
475
476
477
478
479
480
481
482
483
484
485
486
487
488
489
490
491
492
493
494
495
496
497
498
499
500
501
502
503
504
505
506
507
508
509
510
511
512
513
514
515
516
517
518
519
520
521
522
523
524
525
526
527
528
529
530
531
532
533
534
535
536
537
538
539
540
541
542
543
544
545
546
547
548
549
550
551
552
553
554
555
556
557
558
559
560
561
562
563
564
565
566
567
568
569
570
571
572
573
574
575
576
577
578
579
580
581
582
583
584
585
586
587
588
589
590
591
592
593
594
595
596
597
598
599
600
601
602
603
604
605
606
607
608
609
610
611
612
613
614
615
616
617
618
619
620
621
622
623
624
625
626
627
628
629
630
631
632
633
634
635
636
637
638
639
640
641
642
643
644
645
646
647
648
649
650
651
652
653
654
655
656
657
658
659
660
661
662
663
664
665
666
667
668
669
670
671
672
673
674
675
676
677
678
679
680
681
682
683
684
685
686
687
688
689
690
691
692
693
694
695
696
697
698
699
700
701
702
703
704
705
706
707
708
709
710
711
712
713
714
715
716
717
718
719
720
721
722
723
724
725
726
727
728
729
730
731
732
733
734
735
736
737
738
739
740
741
742
743
744
745
746
747
748
749
750
751
752
753
754
755
756
757
758
759
760
761
762
763
764
765
766
767
768
769
770
771
772
773
774
775
776
777
778
779
780
781
782
783
784
785
786
787
788
789
790
791
792
793
794
795
796
797
798
799
800
801
802
803
804
805
806
807
808
809
810
811
812
813
814
815
816
817
818
819
820
821
822
823
824
825
826
827
828
829
830
831
832
833
834
835
836
837
838
839
840
841
842
843
844
845
846
847
848
849
850
851
852
853
854
855
856
857
858
859
860
861
862
863
864
865
866
867
868
869
870
871
872
873
874
875
876
877
878
879
880
881
882
883
884
885
886
887
888
889
890
891
892
893
894
895
896
897
898
899
900
901
902
903
904
905
906
907
908
909
910
911
912
913
914
915
916
917
918
919
920
921
922
923
924
925
926
927
928
929
930
931
932
933
934
935
936
937
938
939
940
941
942
943
944
945
946
947
948
949
950
951
952
953
954
955
956
957
958
959
960
961
962
963
964
965
966
967
968
969
970
971
972
973
974
975
976
977
978
979
980
981
982
983
984
985
986
987
988
989
990
991
992
993
994
995
996
997
998
999
1000

1
2
3
4 15 mL). The combined organics were dried over sodium sulfate and the solvent was
5
6
7 removed under reduced pressure. Product **3** was crystallized from *n*-hexane and ethyl
8
9
10 acetate. White solid; 73% yield; mp. 143–145 °C; ¹H-NMR (400 MHz, DMSO-*d*₆) δ 8.45
11
12 (t, *J* = 5.4 Hz, 1H, NH), 8.02 (d, *J* = 7.4 Hz, 1H, NH), 7.83 – 7.67 (t, *J* = 5.4 Hz, 1H, NH),
13
14 7.37 – 7.22 (m, 5H, arom. H), 6.91 (d, *J* = 6.9 Hz, NH), 4.36 – 4.19 (m, 4H, CH, CH, CH₂),
15
16 2.93 – 2.76 (m, 2H, CH₂), 2.75 – 2.57 (m, 2H, CH₂), 1.36 (s, 9H, ^tBu), 1.24 (d, *J* = 7.0 Hz,
17
18 3H, CH₃), 0.80 (s, 9H, ^tBu) ppm; ¹³C-NMR (101 MHz, DMSO-*d*₆) δ 172.0, 171.0, 169.6,
19
20 155.0, 139.3, 128.2, 127.0, 126.7, 78.2, 51.5, 49.7, 48.4, 42.0, 37.7, 31.9, 28.1, 27.2, 18.2
21
22 ppm; HRMS (m/z): M⁻ calcd. for C₂₄H₃₇N₄O₅, 461.2769; found, 461.2755.
23
24
25
26
27
28
29
30
31
32
33

34
35
36 **(*S*)-2-Amino-*N*'-((*S*)-1-(benzylamino)-1-oxopropan-2-yl)-*N*'-neopentylsuccinamide (**4**).**
37

38
39 Compound **3** (340 mg, 0.73 mmol, 1 eq) was dissolved in a mixture of trifluoroacetic
40
41 acid/CH₂Cl₂ (1:2.25, 13 mL) and stirred at room temperature for 4 h. After completion of
42
43 the reaction, the mixture was basified (pH ≈ 9) using sat. sodium carbonate solution. The
44
45 resulting solution was extracted with CH₂Cl₂ (3 x 20 mL) and washed with brine (1 x 10
46
47 mL). The collected organics were dried over magnesium sulfate and the solvent was
48
49
50
51
52
53
54
55
56
57
58
59
60

1
2
3 removed under reduced pressure. The crude product was recrystallized from methanol
4
5
6
7 and diethyl ether to yield compound **4**. White solid; 75% yield; mp. 160–163 °C; ¹H-NMR
8
9
10 (400 MHz, DMSO-*d*₆) δ 8.49 (t, *J* = 5.8 Hz, 1H, NH), 8.32 (d, *J* = 6.5 Hz, 1H, NH), 7.97 (t,
11
12
13 *J* = 5.6 Hz, 1H, NH), 7.36 – 7.15 (m, 5H, arom. H), 4.35 – 4.11 (m, 3H, CH, CH₂), 3.70 –
14
15
16
17 3.61 (m, 1H, CH), 2.84 (d, *J* = 6.2 Hz, 2H, CH₂), 2.68 – 2.53 (m, 2H, CH₂), 1.26 (d, *J* =
18
19
20
21 7.1 Hz, 3H, CH₃), 0.81 (s, 9H, ^tBu) ppm; ¹³C-NMR (75 MHz, DMSO-*d*₆) δ 172.0, 171.9,
22
23
24 170.1, 169.9, 139.3, 128.2, 127.0, 126.7, 51.1, 49.7, 48.3, 42.0, 31.8, 27.2, 18.3 ppm;
25
26
27
28 HRMS (m/z): MNa⁺ calcd. for C₁₉H₃₀N₄NaO₃, 385.2210; found, 385.2210.
29
30
31

32 ***N*'-((*S*)-1-(((*S*)-1-(Benzylamino)-1-oxopropan-2-yl)amino)-4-(neopentylamino)-1,4-**
33
34
35 **dioxobutan-2-yl)-*N*'-(benzyloxy)terephthalamide (**5**).** A mixture of compound **4** (95 mg,
36
37
38 0.26 mmol, 1 eq), ((benzyloxy)carbonyl)benzoic acid (84 mg, 0.31 mmol, 1.2 eq) and
39
40
41
42 HATU (118 mg, 0.31 mmol, 1.2 eq) was suspended in DMF (3 mL) and
43
44
45
46 diisopropylethylamine (53 μL, 0.31 mmol, 1.2 eq) was added. The resulting solution was
47
48
49
50 stirred at room temperature for 24 h. After completion of the reaction, the solvent was
51
52
53
54 removed under reduced pressure and the remaining solid was washed with sat. sodium
55
56
57
58
59
60

bicarbonate solution (2 x 15 mL), 10% HCl (2 x 15 mL) and diethyl ether (2 x 15 mL). The

crude product was recrystallized from methanol and diethyl ether to yield compound **5**.

White solid; 65% yield; mp. 232–236 °C; ¹H-NMR (400 MHz, DMSO-*d*₆): δ 11.90 (s, 1H,

NH), 8.70 (d, *J* = 7.6 Hz, 1H, NH), 8.43 (t, *J* = 6.1 Hz, 1H, NH), 8.25 (d, *J* = 7.4 Hz, 1H,

NH), 7.94 – 7.87 (m, 2H, arom. H), 7.84 – 7.78 (m, 2H, arom. H), 7.48 – 7.17 (m, 10H,

arom. H), 4.94 (s, 1H, OCH₂), 4.82 – 4.73 (m, 1H, CH), 4.34 – 4.19 (m, 3H, CH₂, CH),

2.89 – 2.63 (m, 4H, CH₂, CH₂), 1.26 (d, *J* = 7.1 Hz, 3H, CH₃), 0.78 (s, 9H, ^tBu) ppm; ¹³C-

NMR (101 MHz, DMSO-*d*₆): δ 172.0, 170.7, 169.7, 165.4, 163.7, 139.4, 136.5, 135.8,

134.7, 129.0, 128.4, 128.2, 127.6, 127.1, 127.0, 126.7, 77.1, 50.9, 49.7, 48.6, 42.0, 37.5,

31.9, 27.2, 18.0 ppm; HRMS (*m/z*): *M*⁻ calcd. for C₃₄H₄₀N₅O₆, 614.2984; found, 614.2979.

***N'*-((*S*)-1-(((*S*)-1-(Benzylamino)-1-oxopropan-2-yl)amino)-4-(neopentylamino)-1,4-dioxobutan-2-yl)-*M*⁴-hydroxyterephthalamide (RTS-V5).** Compound **5** (50 mg, 0.08 mmol,

1 eq) was dissolved in 5 mL MeOH and Pd(C) (5 mg, 10% wt, 4.70 μmol, 0.06 eq) was

added. The mixture was stirred under hydrogen atmosphere at room temperature for 4 h.

After completion of the reaction, the mixture was filtered over celite. The solvent was

1
2
3 removed under reduced pressure and the product RTS-V5 was crystallized from *n*-
4
5
6 hexane and ethyl acetate. White solid; 98% yield; mp. 220 °C (decomp.); t_R : 10.67 min,
7
8
9
10 purity: 95%; $^1\text{H-NMR}$ (500 MHz, $\text{DMSO-}d_6$): δ 11.31 (bs, 1H, OH), 9.10 (bs, 1H, NH), 8.67
11
12
13 (d, $J = 7.6$ Hz, 1H, NH), 8.40 (t, $J = 5.8$ Hz, 1H, NH), 8.20 (d, $J = 7.3$ Hz, 1H, NH), 7.91 –
14
15
16 7.87 (m, 2H, arom. H), 7.84 – 7.80 (m, 2H, arom. H), 7.32 – 7.19 (m, 5H, arom. H), 4.83
17
18
19 – 4.72 (m, 1H, CH), 4.34 – 4.21 (m, 3H, CH_2 , CH), 2.91 – 2.79 (m, 2H, CH_2), 2.77 – 2.63
20
21
22 (m, 2H, CH_2), 1.26 (d, $J = 7.1$ Hz, 3H, CH_3), 0.78 (s, 9H, $t\text{Bu}$) ppm; $^{13}\text{C-NMR}$ (126 MHz,
23
24
25
26
27 $\text{DMSO-}d_6$): δ 171.9, 170.5, 169.6, 165.5, 139.2, 136.0, 135.2, 128.1, 127.3, 126.9, 126.7,
28
29
30
31 126.6, 50.9, 49.7, 48.5, 42.0, 37.4, 31.7, 27.1, 17.9 ppm; HRMS (m/z): MH^+ calcd. for
32
33
34 $\text{C}_{27}\text{H}_{36}\text{N}_5\text{O}_6$, 526.2660; found, 526.2669.

35 36 37 38 39 **Biological evaluation**

40
41
42
43
44 *Cell culture.* SEM, HL60, KCL22, K562 leukemic cell lines were cultured in RPMI1640
45
46
47 supplemented with 10% FCS and maintained at 37°C with 5% CO_2 , except for SUP-B15
48
49
50 (BCR-ABL1) BCP-ALL cell line which was cultured in McCoy's 5A supplemented with
51
52
53
54 20% of FCS (DSMZ, Braunschweig, Germany). Mononuclear cells (MNC) were isolated
55
56
57
58
59
60

1
2
3
4 by Ficoll density gradient centrifugation using standard procedures and later cultured in
5
6
7 Mononuclear Cell Medium (PromoCell, Heidelberg, Germany). CD34+ cells were later
8
9
10 sorted from these MNC using MACS (Miltenyi Biotec, Bergisch Gladbach, Germany).
11
12
13
14 Primary patient samples were obtained from newly diagnosed patients or from relapse
15
16
17 after informed consent approval of the local ethics committee and were cultured either in
18
19
20 Stemline® II Hematopoietic Stem Cell Expansion Medium (Sigma-Aldrich) or in
21
22
23
24 Mononuclear Cell Medium (PromoCell)
25
26
27

28
29 *CellTiter-Glo® luminescent cell viability assay.* CellTiter-Glo® Luminescent Cell
30
31
32 Viability Assay (Promega, Madison, USA) was performed to determine the IC₅₀ values for
33
34
35 every cell line. Inhibitors were printed on white 384-well plates (Thermo Fisher Scientific,
36
37
38 Waltham, USA) with increasing concentrations (50 nM-25 µM) by using a digital
39
40
41 dispenser (D300e, Tecan, Männedorf, Switzerland). Cell viability was monitored after
42
43
44 72 h using CellTiter-Glo luminescent assay using a Microplate reader (Spark®, Tecan).
45
46
47
48
49
50 IC₅₀ for the compounds were determined by plotting raw data (normalized to controls)
51
52
53
54
55
56
57
58
59
60

1
2
3 using sigmoid dose curve and non-linear regression (GraphPad Prism Inc., San Diego,
4
5
6
7 CA).

10
11 *Proteasome activity assay.* To analyze if treatment with RTS-V5 leads to decreased
12
13
14
15 proteasome activity, chymotrypsin-like, trypsin-like, and caspase-like protease activities
16
17
18 associated with the proteasome complex were measured. Therefore, Cell-Based
19
20
21
22 Proteasome-Glo™ assay kits (Promega, Madison, USA) were used which contain
23
24
25
26
27
28
29
30
31
32
33
34
35
36
37
38
39
40
41
42
43
44
45
46
47
48
49
50
51
52
53
54
55
56
57
58
59
60
luminogenic substrates that are recognized and cleaved by the proteasome into
aminoluciferin. Aminoluciferin is consumed by Ultra-Glo™ luciferase, producing a
luminescent signal correlating to proteasome activity. Luminescence was measured
afterwards using a Microplate reader (Spark®, Tecan).

40
41 *Caspase assay.* Caspase-Glo® 3/7 assay was used to show the impact of the inhibitors
42
43
44
45
46
47
48
49
50
51
52
53
54
55
56
57
58
59
60
on the activity of caspase-3 and -7 in the cells. Caspase-3 and -7 are key players in
apoptosis. The kit contains a luminogenic substrate of caspase-3 and -7 with a DEVD
sequence. This sequence can be recognized and cleaved by caspase-3 and -7. The
cleavage results in a luminescent signal which is proportional to the amount of caspase

1
2
3 activity. Cells were seeded and treated with the IC₅₀ or 2x IC₅₀ concentrations of the
4
5
6
7 inhibitors for 48 h and later the luminescence was measured with a Microplate reader
8
9
10 (Spark®, Tecan).

11
12
13
14
15 *Proliferation assay.* To investigate the influence of the inhibitors on the proliferation,
16
17
18 cells were counted after every 24 h interval through trypan exclusion method using
19
20
21
22 automated cell counter (Vi-CELL™ XR -Beckman Coulter).

23
24
25
26 *Annexin V staining.* For evaluating apoptosis, cells treated with respective compounds
27
28
29 or control for 48 h were stained with Annexin V and PI and later subjected to FACS,
30
31
32
33 following supplier's guidelines (Invitrogen, Carlsbad, CA, USA).

34
35
36
37
38 *Cell cycle analysis.* To investigate if cells treated with the inhibitors show differences in
39
40
41 the cell cycle progression as compared to untreated cells, cell cycle analysis was
42
43
44 performed. Therefore, cells were permeabilized and DNA was stained with PI which binds
45
46
47
48 stoichiometric, i.e. proportional to the amount of DNA present in the cell. Fluorescence
49
50
51 was measured by flow cytometry with FACSCalibur (Becton Dickinson, Heidelberg,
52
53
54
55 Germany).

1
2
3
4 *Western blotting.* Cell lysates were generated after 24 h treatment with the respective
5
6
7 inhibitors and later immunoblotted using anti-PARP (# 9542), anti-Acetyl- α -tubulin
8
9
10 (# 5335), anti-Histone H3 (# 9677), anti-HSP90 (# 4877), anti-Grp94 (# 2104), anti-HSF-
11
12
13 1 (# 4356), anti-HSP70 (# 4872), anti-PDI (# 2446), anti-HSP60 (# 12165), anti-HSP40
14
15
16 (# 4871), anti-pHSP27 (# 9709), anti-HSP27 (# 2402), anti-BIP (# 3177), anti-ATF6
17
18
19 (# 65880), anti-ATF4 (# 11815), anti-pMAPK (# 4370), anti-MAPK (# 4695), anti-pJNK
20
21
22 (# 4668), anti-JNK (# 9252), anti-p62 (# 5114), anti-LC3B (# 3868) and anti-GAPDH
23
24
25 (# 2118) (Cell Signaling Technology, Danvers, MA).
26
27
28
29
30

31
32 *Differentiation assay.* Healthy cells differentiate into specialized cells when they mature.
33
34
35
36 In contrast, cancer cells remain undifferentiated or poorly differentiated to maintain their
37
38
39 ability of fast replication. Differentiation assay was performed to analyze if treatment with
40
41
42 the inhibitors leads to increased differentiation of the cells. Therefore, antibodies against
43
44
45 specific surface molecules that cells express depending on their stage of differentiation
46
47
48
49 were used as differentiation markers. FACS was performed on FACSCalibur (Becton
50
51
52
53 Dickinson, Heidelberg, Germany) by using fluorochrome coupled monoclonal antibodies
54
55
56
57
58
59
60

1
2
3 (mAbs) along with matched isotype controls: anti-CD11b (Bear1) and anti-CD14 (RMO52)
4
5
6
7 (Beckman Coulter).
8
9

10
11 *CFU assay.* Colony forming unit assays (CFU) were performed initially treating the cells
12
13
14 in the liquid medium for 24 h and later the treated cells were seeded in the semisolid
15
16
17 methylcellulose-based medium containing respective compounds or control. Colonies
18
19
20
21
22 were counted after 14 days.
23
24
25

26 *Aggresome detection assay.* As RTS-V5 simultaneously blocks the 20S proteasome
27
28
29 and HDAC6 we planned to evaluate its effect on aggresome production using a proteostat
30
31
32 aggresome detection kit (Enzo Life Sciences). Cells were labeled using an aggresome
33
34
35
36
37 detection kit following the manufacturer's guidelines. After 18 h treatment with the
38
39
40
41
42
43
44
45
46
47
48
49
50
51
52
53
54
55
56
57
58
59
60
61
62
63
64
65
66
67
68
69
70
71
72
73
74
75
76
77
78
79
80
81
82
83
84
85
86
87
88
89
90
91
92
93
94
95
96
97
98
99
100
101
102
103
104
105
106
107
108
109
110
111
112
113
114
115
116
117
118
119
120
121
122
123
124
125
126
127
128
129
130
131
132
133
134
135
136
137
138
139
140
141
142
143
144
145
146
147
148
149
150
151
152
153
154
155
156
157
158
159
160
161
162
163
164
165
166
167
168
169
170
171
172
173
174
175
176
177
178
179
180
181
182
183
184
185
186
187
188
189
190
191
192
193
194
195
196
197
198
199
200
201
202
203
204
205
206
207
208
209
210
211
212
213
214
215
216
217
218
219
220
221
222
223
224
225
226
227
228
229
230
231
232
233
234
235
236
237
238
239
240
241
242
243
244
245
246
247
248
249
250
251
252
253
254
255
256
257
258
259
260
261
262
263
264
265
266
267
268
269
270
271
272
273
274
275
276
277
278
279
280
281
282
283
284
285
286
287
288
289
290
291
292
293
294
295
296
297
298
299
300
301
302
303
304
305
306
307
308
309
310
311
312
313
314
315
316
317
318
319
320
321
322
323
324
325
326
327
328
329
330
331
332
333
334
335
336
337
338
339
340
341
342
343
344
345
346
347
348
349
350
351
352
353
354
355
356
357
358
359
360
361
362
363
364
365
366
367
368
369
370
371
372
373
374
375
376
377
378
379
380
381
382
383
384
385
386
387
388
389
390
391
392
393
394
395
396
397
398
399
400
401
402
403
404
405
406
407
408
409
410
411
412
413
414
415
416
417
418
419
420
421
422
423
424
425
426
427
428
429
430
431
432
433
434
435
436
437
438
439
440
441
442
443
444
445
446
447
448
449
450
451
452
453
454
455
456
457
458
459
460
461
462
463
464
465
466
467
468
469
470
471
472
473
474
475
476
477
478
479
480
481
482
483
484
485
486
487
488
489
490
491
492
493
494
495
496
497
498
499
500
501
502
503
504
505
506
507
508
509
510
511
512
513
514
515
516
517
518
519
520
521
522
523
524
525
526
527
528
529
530
531
532
533
534
535
536
537
538
539
540
541
542
543
544
545
546
547
548
549
550
551
552
553
554
555
556
557
558
559
560
561
562
563
564
565
566
567
568
569
570
571
572
573
574
575
576
577
578
579
580
581
582
583
584
585
586
587
588
589
590
591
592
593
594
595
596
597
598
599
600
601
602
603
604
605
606
607
608
609
610
611
612
613
614
615
616
617
618
619
620
621
622
623
624
625
626
627
628
629
630
631
632
633
634
635
636
637
638
639
640
641
642
643
644
645
646
647
648
649
650
651
652
653
654
655
656
657
658
659
660
661
662
663
664
665
666
667
668
669
670
671
672
673
674
675
676
677
678
679
680
681
682
683
684
685
686
687
688
689
690
691
692
693
694
695
696
697
698
699
700
701
702
703
704
705
706
707
708
709
710
711
712
713
714
715
716
717
718
719
720
721
722
723
724
725
726
727
728
729
730
731
732
733
734
735
736
737
738
739
740
741
742
743
744
745
746
747
748
749
750
751
752
753
754
755
756
757
758
759
760
761
762
763
764
765
766
767
768
769
770
771
772
773
774
775
776
777
778
779
780
781
782
783
784
785
786
787
788
789
790
791
792
793
794
795
796
797
798
799
800
801
802
803
804
805
806
807
808
809
810
811
812
813
814
815
816
817
818
819
820
821
822
823
824
825
826
827
828
829
830
831
832
833
834
835
836
837
838
839
840
841
842
843
844
845
846
847
848
849
850
851
852
853
854
855
856
857
858
859
860
861
862
863
864
865
866
867
868
869
870
871
872
873
874
875
876
877
878
879
880
881
882
883
884
885
886
887
888
889
890
891
892
893
894
895
896
897
898
899
900
901
902
903
904
905
906
907
908
909
910
911
912
913
914
915
916
917
918
919
920
921
922
923
924
925
926
927
928
929
930
931
932
933
934
935
936
937
938
939
940
941
942
943
944
945
946
947
948
949
950
951
952
953
954
955
956
957
958
959
960
961
962
963
964
965
966
967
968
969
970
971
972
973
974
975
976
977
978
979
980
981
982
983
984
985
986
987
988
989
990
991
992
993
994
995
996
997
998
999
1000

HDAC IC₅₀ profiling. The in vitro inhibitory activity of RTS-V5 against five human HDAC isoforms (1, 2, 3, 6, and 8) were determined at Reaction Biology Corp. (Malvern, PA) with a fluorescence-based assay according to the company's standard operating procedure

1
2
3 using RHKK(Ac)AMC (HDACs 1, 2, 3, and 6) or RHK(Ac)K(Ac)AMC (HDAC8) as
4
5
6
7 substrates. The IC_{50} values were determined in duplicate using 10 different
8
9
10 concentrations with 3-fold serial dilution starting at 100 μ M. TSA (HDAC1 IC_{50} : 9.4 nM,
11
12
13 HDAC2 IC_{50} : 26.7 nM, HDAC₃ IC_{50} : 12.7 nM, HDAC6 IC_{50} : 8.5 nM, and HDAC8 IC_{50} : 609
14
15
16
17 nM) was used as reference compound.
18
19
20
21

22 X-ray crystallography

23
24
25

26 Experimental details for the X-ray crystal structure determination of HDAC6 and the
27
28
29 yeast 20S proteasome in complex with RTS-V5 can be found in the Supporting
30
31
32
33 Information.
34
35
36
37

38 ASSOCIATED CONTENT

39
40
41

42 **Supporting Information.** This material is available free of charge via the Internet at
43
44
45
46 <http://pubs.acs.org>.
47
48
49
50
51
52
53
54
55
56
57
58
59
60

1
2
3
4 Supplementary Figures and Tables, experimental procedures, compound
5
6
7 characterization data, X-ray crystallography, HPLC traces and NMR spectra of newly
8
9
10 synthesized compounds.

11
12
13
14
15 Molecular Formula Strings and some data (CSV).

16
17
18
19
20 **Accession codes.** Protein Data Bank (PDB): HDAC6–RTS-V5 complex, 6CW8;
21
22
23 Proteasome–RTS-V5 complex, 6H39. Authors will release the atomic coordinates and
24
25
26
27 experimental data upon article publication.

28 29 30 31 32 33 34 **AUTHOR INFORMATION**

35 36 37 38 **Corresponding Author**

39
40
41
42 * Phone: (+49) 341 97 36801, Fax (+49) 341 97 36889, E-mail: finn.hansen@medizin.uni-
43
44
45 leipzig.de

46
47
48
49 * Phone: (+49) 211 81 17680, Fax (+49) 211 81 16206, E-mail: julia.hauer@med.uni-
50
51
52 duesseldorf.de

Author Contributions

The manuscript was written through contributions of all authors. All authors have given approval to the final version of the manuscript.

‡ These authors contributed equally to this work as first authors.

§ These authors contributed equally to this work as senior authors.

Notes

The authors declare no competing financial interest.

ACKNOWLEDGMENT

We thank Nicholas Porter for helpful scientific discussions. Additionally, we thank Alexei Soares and the beamline staff at the National Synchrotron Light Source II (NSLS-II) for assistance with data collection using AMX beamline 17-ID-1. NSLS-II is a U.S. Department of Energy (DOE) Office of Science User Facility operated by Brookhaven National Laboratory under Contract No. DE-SC0012704. We are grateful to the staff of the beamline X06SA at the Paul-Scherrer-Institute, Swiss Light Source, Villigen

1
2
3 (Switzerland), for assistance during data collection of the proteasome complex. Richard
4
5
6
7 Feicht is acknowledged for the purification and crystallization of the yeast 20S core
8
9
10
11 particle. Experimental support from Alexandra Herrlich is gratefully appreciated. This
12
13
14 research was financially supported by NIH Grant GM49758 (to D.W.C) and by the
15
16
17 Deutsche Forschungsgemeinschaft (SFB1035, to M.G.). F.K.H. acknowledges financial
18
19
20 support from the Fonds der Chemischen Industrie (FCI). J.H. has been supported by the
21
22
23
24 German Children's Cancer Foundation (Project 110997 and Translational Oncology
25
26
27 Program 70112951), the German Carreras Foundation (DJCLS 02R/2016), the
28
29
30
31 Kinderkrebsstiftung (2016/17) and the Elterninitiative Kinderkrebsklinik e.V. Düsseldorf.
32
33
34
35 S.B. acknowledges the financial support by Forschungskommission, HHU (2018-04).
36
37
38
39
40
41

42 **ABBREVIATIONS USED**

43
44
45

46 CFU, colony forming assay; DMSO, dimethylsulfoxide; HDAC, histone deacetylase;
47
48
49 HDAC6 CD2, histone deacetylase 6 catalytic domain 2; PI, proteasome inhibitor; AML,
50
51
52 acute myeloid leukemia; BCP-ALL, B-cell precursor acute lymphoblastic leukemia; CML,
53
54
55
56
57
58
59
60

1
2
3 chronic myeloid leukemia; MM, multiple myeloma; TKI, tyrosine kinase inhibitor; PARP,
4
5
6 poly(ADP-ribose) polymerase; PBMCs, peripheral blood derived mononuclear cells;
7
8
9
10 HSR, heat shock response; UPR, unfolded protein response.
11
12
13

14 REFERENCES

- 15
16
17
18
19 (1) Anighoro, A.; Bajorath, J.; Rastelli, G. Polypharmacology: challenges and
20
21
22 opportunities in drug discovery. *J. Med. Chem.* **2014**, *57*, 7874-7887.
23
24
25
26 (2) Roche, J.; Bertrand, P. Inside HDACs with more selective HDAC inhibitors. *Eur. J.*
27
28
29 *Med. Chem.* **2016**, *121*, 451-483.
30
31
32
33 (3) Maolanon, A. R.; Kristensen, H. M.; Leman, L. J.; Ghadiri, M. R.; Olsen, C. A.
34
35
36 Natural and synthetic macrocyclic inhibitors of the histone deacetylase enzymes.
37
38
39 *ChemBioChem* **2017**, *18*, 5-49.
40
41
42
43 (4) (a) Ganesan, A. Multitarget Drugs: an Epigenetic Epiphany. *ChemMedChem*
44
45
46 **2016**, *11*, 1227-1241; (b) de Lera, A. R.; Ganesan, A. Epigenetic
47
48
49 polypharmacology: from combination therapy to multitargeted drugs. *Clin.*
50
51
52
53
54 *Epigenetics* **2016**, *8*, 105.
55
56
57
58
59
60

- 1
2
3
4 (5) (a) Millard, C. J.; Watson, P. J.; Fairall, L.; Schwabe, J. W. R. Targeting class I
5
6
7 histone deacetylases in a "complex" environment. *Trends Pharmacol. Sci.* **2017**,
8
9
10 *38*, 363-377; (b) Schobert, R.; Biersack, B. Multimodal HDAC inhibitors with
11
12
13 improved anticancer activity. *Curr. Cancer Drug Targets* **2018**, *18*, 39-56.
14
15
16
17 (6) Hideshima, T.; Richardson, P. G.; Anderson, K. C. Mechanism of action of
18
19
20 proteasome inhibitors and deacetylase inhibitors and the biological basis of
21
22
23 synergy in multiple myeloma. *Mol. Cancer Ther.* **2011**, *10*, 2034-2042.
24
25
26
27 (7) Beck, P.; Dubiella, C.; Groll, M. Covalent and non-covalent reversible proteasome
28
29
30 inhibition. *Biol. Chem.* **2012**, *393*, 1101-1120.
31
32
33
34 (8) Gallastegui, N.; Beck, P.; Arciniega, M.; Huber, R.; Hillebrand, S.; Groll, M.
35
36
37 Hydroxyureas as noncovalent proteasome inhibitors. *Angew. Chem. Int. Ed.* **2012**,
38
39
40
41 *51*, 247-249.
42
43
44 (9) Groll, M.; Koguchi, Y.; Huber, R.; Kohno, J. Crystal structure of the 20 S
45
46
47 proteasome:TMC-95A complex: a non-covalent proteasome inhibitor. *J. Mol. Biol.*
48
49
50
51 **2001**, *311*, 543-548.
52
53
54
55
56
57
58
59
60

- 1
2
3
4 (10) (a) Kaiser, M.; Groll, M.; Siciliano, C.; Assfalg-Machleidt, I.; Weyher, E.; Kohno, J.;
5
6
7 Milbradt, A. G.; Renner, C.; Huber, R.; Moroder, L. Binding mode of TMC-95A
8
9
10 analogues to eukaryotic 20S proteasome. *ChemBioChem* **2004**, *5*, 1256-1266; (b)
11
12
13 Groll, M.; Gotz, M.; Kaiser, M.; Weyher, E.; Moroder, L. TMC-95-based inhibitor
14
15
16 design provides evidence for the catalytic versatility of the proteasome. *Chemistry*
17
18
19 & *biology* **2006**, *13*, 607-614; (c) Desvergne, A.; Genin, E.; Marechal, X.;
20
21
22 Gallastegui, N.; Dufau, L.; Richy, N.; Groll, M.; Vidal, J.; Reboud-Ravaux, M.
23
24
25 Dimerized linear mimics of a natural cyclopeptide (TMC-95A) are potent
26
27
28 noncovalent inhibitors of the eukaryotic 20S proteasome. *J. Med. Chem.* **2013**, *56*,
29
30
31
32
33
34
35 3367-3378.
36
37
38 (11) (a) Blackburn, C.; Gigstad, K. M.; Hales, P.; Garcia, K.; Jones, M.; Bruzzese, F. J.;
39
40
41 Barrett, C.; Liu, J. X.; Soucy, T. A.; Sappal, D. S.; Bump, N.; Olhava, E. J.; Fleming,
42
43
44 P.; Dick, L. R.; Tsu, C.; Sintchak, M. D.; Blank, J. L. Characterization of a new
45
46
47 series of non-covalent proteasome inhibitors with exquisite potency and selectivity
48
49
50
51 for the 20S β 5-subunit *Biochem. J.* **2010**, *430*, 461-476; (b) Groll, M.; Gallastegui,
52
53
54
55 N.; Marechal, X.; Le Ravalec, V.; Basse, N.; Richy, N.; Genin, E.; Huber, R.;
56
57
58
59
60

- 1
2
3
4 Moroder, L.; Vidal, J.; Reboud-Ravaux, M. 20S proteasome inhibition: designing
5
6
7 noncovalent linear peptide mimics of the natural product TMC-95A.
8
9
10 *ChemMedChem* **2010**, *5*, 1701- 1705.
11
12
13
14 (12) Huber, E. M.; Groll, M. Inhibitors for the immuno- and constitutive proteasome:
15
16
17 current and future trends in drug development. *Angew. Chem. Int. Ed.* **2012**, *51*,
18
19
20 8708-8720.
21
22
23
24 (13) Hideshima, T.; Qi, J.; Paranal, R. M.; Tang, W.; Greenberg, E.; West, N.; Colling,
25
26
27 M. E.; Estiu, G.; Mazitschek, R.; Perry, J. A.; Ohguchi, H.; Cottini, F.; Mimura, N.;
28
29
30 Gorgun, G.; Tai, Y. T.; Richardson, P. G.; Carrasco, R. D.; Wiest, O.; Schreiber,
31
32
33
34 S. L.; Anderson, K. C.; Bradner, J. E. Discovery of selective small-molecule
35
36
37 HDAC6 inhibitor for overcoming proteasome inhibitor resistance in multiple
38
39
40
41 myeloma. *Proc. Natl. Acad. Sci. USA* **2016**, *113*, 13162-13167.
42
43
44
45 (14) (a) Olson, D. E.; Wagner, F. F.; Kaya, T.; Gale, J. P.; Aidoud, N.; Davoine, E. L.;
46
47
48 Lazzaro, F.; Weiwer, M.; Zhang, Y. L.; Holson, E. B. Discovery of the first histone
49
50
51 deacetylase 6/8 dual inhibitors. *J. Med. Chem.* **2013**, *56*, 4816-4820; (b) Wagner,
52
53
54
55 F. F.; Olson, D. E.; Gale, J. P.; Kaya, T.; Weiwer, M.; Aidoud, N.; Thomas, M.;
56
57
58
59
60

- 1
2
3
4 Davoine, E. L.; Lemercier, B. C.; Zhang, Y.-L.; Holson, E. B. Potent and selective
5
6
7 inhibition of histone deacetylase 6 (HDAC6) does not require a surface-binding
8
9
10 motif. *J. Med. Chem.* **2013**, *56*(4), 1772–1776.
11
12
13
14 (15) Miyake, Y.; Keusch, J. J.; Wang, L.; Saito, M.; Hess, D.; Wang, X.; Melancon, B.
15
16
17 J.; Helquist, P.; Gut, H.; Matthias, P. Structural insights into HDAC6 tubulin
18
19
20 deacetylation and its selective inhibition. *Nat. Chem. Biol.* **2016**, *12*, 748-754.
21
22
23
24 (16) Bhatia, S.; Diedrich, D.; Frieg, B.; Ahlert, H.; Stein, S.; Bopp, B.; Lang, F.; Zang,
25
26
27 T.; Kroger, T.; Ernst, T.; Kogler, G.; Krieg, A.; Ludeke, S.; Kunkel, H.; Rodrigues
28
29
30 Moita, A. J.; Kassack, M. U.; Marquardt, V.; Opitz, F. V.; Oldenburg, M.; Remke,
31
32
33 M.; Babor, F.; Grez, M.; Hochhaus, A.; Borkhardt, A.; Groth, G.; Nagel-Steger, L.;
34
35
36 Jose, J.; Kurz, T.; Gohlke, H.; Hansen, F. K.; Hauer, J. Targeting HSP90
37
38
39 dimerization via the C-terminus is effective in imatinib resistant CML and lacks the
40
41
42 heat shock response. *Blood* **2018**, *132*, 307–320.
43
44
45
46
47
48 (17) (a) Hai, Y.; Christianson, D. W. Histone deacetylase 6 structure and molecular
49
50
51 basis of catalysis and inhibition. *Nat. Chem. Biol.* **2016**, *12*, 741-747; (b) Porter, N.
52
53
54
55 J.; Mahendran, A.; Breslow, R.; Christianson, D. W. Unusual zinc-binding mode of
56
57
58
59
60

- 1
2
3 HDAC6-selective hydroxamate inhibitors. *Proc. Natl. Acad. Sci. USA* **2017**, *114*,
4
5
6
7 13459-13464; (c) Mackwitz, M. K. W.; Hamacher, A.; Osko, J. D.; Held, J.; Schöler,
8
9
10 A.; Christianson, D. W.; Kassack, M. U.; Hansen, F. K. Multicomponent Synthesis
11
12 and binding mode of imidazo[1,2-*a*]pyridine-capped selective HDAC6 inhibitors.
13
14
15
16
17 *Org. Lett.* **2018**, *20*, 3255–3258. (d) Porter, N. J.; Osko, J. D.; Diedrich, D.; Kurz,
18
19
20 T.; Hooker, J. M.; Hansen, F. K.; Christianson, D. W. Histone deacetylase 6-
21
22 selective inhibitors and the influence of capping groups on hydroxamate-zinc
23
24
25
26
27
28 denticity. *J. Med. Chem.* **2018**, *61*, 8054–8060.
29
30
31 (18) Löwe, J.; Stock, D.; Jap, B.; Zwickl, P.; Baumeister, W.; Huber, R. Crystal structure
32
33
34 of the 20S proteasome from the archaeon *T. acidophilum* at 3.4 Å resolution.
35
36
37
38 *Science* **1995**, *268*, 533-539.
39
40
41 (19) Groll, M.; Ditzel, L.; Lowe, J.; Stock, D.; Bochtler, M.; Bartunik, H. D.; Huber, R.
42
43
44
45 Structure of 20S proteasome from yeast at 2.4 Å resolution. *Nature* **1997**, *386*,
46
47
48
49 463-471.
50
51
52 (20) Stein, M. L.; Cui, H.; Beck, P.; Dubiella, C.; Voss, C.; Kruger, A.; Schmidt, B.; Groll,
53
54
55
56 M. Systematic comparison of peptidic proteasome inhibitors highlights the alpha-
57
58
59
60

- 1
2
3 ketoamide electrophile as an auspicious reversible lead motif. *Angew. Chem. Int.*
4
5
6
7 *Ed.* **2014**, *53*, 1679-1683.
8
9
- (21) Huber, E. M.; Heinemeyer, W.; Li, X.; Arendt, C. S.; Hochstrasser, M.; Groll, M. A
10
11 unified mechanism for proteolysis and autocatalytic activation in the 20S
12
13
14
15
16
17 proteasome. *Nature Commun.* **2016**, *7*, 10900.
18
19
- (22) Borissenko, L.; Groll, M. 20S proteasome and its inhibitors: crystallographic
20
21
22
23
24
25
26
27 knowledge for drug development. *Chem. Rev.* **2007**, *107*, 687-717.
28
- (23) Morphy, R.; Kay, C.; Rankovic, Z. From magic bullets to designed multiple ligands.
29
30
31
32
33
34
35
36
37
38
39
40
41
42
43
44
45
46
47
48
49
50
51
52
53
54
55
56
57
58
59
60
- (24) Bayat Mokhtari, R.; Homayouni, T. S.; Baluch, N; Morgatskaya, E.; Kumar, S.; Das,
B.; Yeger, H. Combination therapy in combating cancer. *Oncotarget* **2017**, *8*,
38022-38043.
- (25) Hideshima, T.; Bradner, J. E.; Wong, J.; Chauhan, D.; Richardson, P.; Schreiber,
S. L.; Anderson, K. C. Small-molecule inhibition of proteasome and aggresome
function induces synergistic antitumor activity in multiple myeloma. *Proc. Natl.*
Acad. Sci. USA **2005**, *102*, 8567-8572.

- 1
2
3
4 (26) Delic, J.; Morange, M.; Magdelenat, H. Ubiquitin pathway involvement in human
5
6
7 lymphocyte gamma-irradiation-induced apoptosis. *Mol. Cell. Biol.* **1993**, *13*, 4875-
8
9
10 4883.
11
12
13
14 (27) Vogl, D. T.; Raje, N.; Jagannath, S.; Richardson, P.; Hari, P.; Orlowski, R.; Supko,
15
16
17 J. G.; Tamang, D.; Yang, M.; Jones, S. S.; Wheeler, C.; Markelewicz, R. J.; Lonial,
18
19
20 S. Ricolinostat, the first selective histone deacetylase 6 inhibitor, in combination
21
22
23 with bortezomib and dexamethasone for relapsed or refractory multiple myeloma.
24
25
26
27
28 *Clin. Cancer Res.* **2017**, *23*, 3307-3315.
29
30
31 (28) Zhou, W.; Zhu, W.; Ma, L.; Xiao, F.; Qian, W. Proteasome inhibitor MG-132
32
33
34 enhances histone deacetylase inhibitor SAHA-induced cell death of chronic
35
36
37 myeloid leukemia cells by an ROS-mediated mechanism and downregulation of
38
39
40
41 the Bcr-Abl fusion protein. *Oncol. Lett.* **2015**, *10*, 2899-2904.
42
43
44
45 (29) Kalin, J. H.; Bergman, J. A. Development and therapeutic implications of selective
46
47
48 histone deacetylase 6 inhibitors. *J. Med. Chem.* **2013**, *56*, 6297-6313.
49
50
51
52

53 Table of Contents graphic
54
55
56
57
58
59
60

